

# Deep Multi-Task Learning for Cooperative NOMA: System Design and Principles

Yuxin Lu, Peng Cheng, Zhuo Chen, Wai Ho Mow, Yonghui Li, and Branka Vucetic

## Abstract

Envisioned as a promising component of the future wireless Internet-of-Things (IoT) networks, the non-orthogonal multiple access (NOMA) technique can support massive connectivity with a significantly increased spectral efficiency. Cooperative NOMA is able to further improve the communication reliability of users under poor channel conditions. However, the conventional system design suffers from several inherent limitations and is not optimized from the bit error rate (BER) perspective. In this paper, we develop a novel deep cooperative NOMA scheme, drawing upon the recent advances in deep learning (DL). We develop a novel hybrid-cascaded deep neural network (DNN) architecture such that the entire system can be optimized in a holistic manner. On this basis, we construct multiple loss functions to quantify the BER performance and propose a novel multi-task oriented two-stage training method to solve the end-to-end training problem in a self-supervised manner. The learning mechanism of each DNN module is then analyzed based on information theory, offering insights into the proposed DNN architecture and its corresponding training method. We also adapt the proposed scheme to handle the power allocation (PA) mismatch between training and inference and incorporate it with channel coding to combat signal deterioration. Simulation results verify its advantages over orthogonal multiple access (OMA) and the conventional cooperative NOMA scheme in various scenarios.

## Index Terms

Cooperative non-orthogonal multiple access, deep learning, multi-task learning, neural network, self-supervised learning

Yuxin Lu and Wai Ho Mow are with the Department of Electronic and Computer Engineering, the Hong Kong University of Science and Technology, Hong Kong S.A.R. (e-mail: ylubg@ust.hk; eewhmow@ust.hk).

Yonghui Li and Branka Vucetic are with the School of Electrical and Information Engineering, the University of Sydney, Australia, (e-mail: yonghui.li@sydney.edu.au; branka.vucetic@sydney.edu.au).

Peng Cheng is with the Department of Computer Science and Information Technology, La Trobe University, Melbourne, VIC 3086, Australia, and also with the School of Electrical and Information Engineering, the University of Sydney, Sydney, NSW 2006, Australia (e-mail: p.cheng@latrobe.edu.au; peng.cheng@sydney.edu.au).

Zhuo Chen is with the CSIRO DATA61, Marsfield, NSW 2122, Australia (e-mail: zhuo.chen@ieee.org).

## I. INTRODUCTION

Massive wireless device connectivity under limited spectrum resources is considered as cornerstone of the wireless Internet-of-Things (IoT) evolution. As a transformative physical-layer technology, non-orthogonal multiple access (NOMA) [1], [2] leverages superposition coding (SC) and successive interference cancellation (SIC) techniques to support simultaneous multiple user transmission in the same time-frequency resource block. Compared with its conventional orthogonal multiple access (OMA) counterpart, NOMA can significantly increase the spectrum efficiency, reduce access latency, and achieve more balanced user fairness [3]. Typically, NOMA functions in either the power domain, by multiplexing different power levels, or the code domain, by utilizing partially overlapping codes [4].

Cooperative NOMA, which integrates cooperative communication techniques into NOMA, can further improve the communication reliability of users under poor channel conditions, and therefore largely extend the radio coverage [5]. Consider a downlink transmission scenario, where there are two classes of users: 1) near users, which have better channel conditions and are usually located close to the base station (BS); and 2) far users, which have worse channel conditions and are usually located close to the cell edge. The near users perform SIC or joint maximum-likelihood (JML) detection to detect their own information, thereby obtaining the prior knowledge of the far users' messages. Then, the near users act as relays and forward the prior information to the far users, thereby improving the reception reliability and reducing the outage probability for the far users. Many novel information-theoretic NOMA contributions have been proposed. It was shown in [6]–[8] that a significant improvement in terms of the outage probability can be achieved, compared to the non-cooperative counterpart. The impact of user pairing on the outage probability and throughput was investigated in [9], where both random and distance-based pairing strategies were analyzed. To address the issue that the near users are energy-constrained, the energy harvesting technique was introduced into cooperative NOMA in [10], where three user selection schemes were proposed and their performances were analyzed.

Different from the information-theoretic approach aforementioned, in this paper, we aim to uplift the performance of cooperative NOMA from the bit error rate (BER) perspective, and provide specific guidance to a practical system design. Our further investigation indicates that the conventional cooperative NOMA suffers from three main limitations (detailed in Section II-B). First, the conventional composite constellation design at the BS adopts a separate mapping rule. Based on a standard constellation such as quadrature amplitude modulation (QAM), bits are first mapped to user symbols, which in turn are mapped into a composite symbol using SC. This results in a reduced minimum Euclidean

distance. Second, while forwarding the far user's signal, the near user does not dynamically design the corresponding constellation [11]–[13], but only reuses the same far user constellation at the BS. Last, the far user treats the near user's interference signal as additive white Gaussian noise (AWGN), which is usually not the case. Besides, it applies maximal-ratio combining (MRC) for signal detection, which ignores the potential error propagation from the near user [11].

These limitations motivate us to develop a novel cooperative NOMA design referred to as deep cooperative NOMA. The essence lies in its holistic approach, taking into account the three limitations simultaneously to perform an end-to-end multi-objective joint optimization. However, this task is quite challenging, because it is intractable to transform the multiple objectives into explicit expressions, not to mention to optimize them simultaneously. To address this challenge, we leverage the interdisciplinary synergy from deep learning (DL) [14]–[21]. We develop a novel hybrid-cascaded deep neural network (DNN) architecture to represent the entire system, and construct multiple loss functions to quantify the BER performance. The DNN architecture consists of several structure-specific DNN modules, capable of tapping the strong capability of universal function approximation and integrating the communication domain knowledge with combined analytical and data-driven modelling.

The remaining task is how to train the proposed DNN architecture through learning the parameters of all the DNN modules in an efficient manner. To handle multiple loss functions, we propose a novel multi-task oriented training method with two stages. In stage I, we minimize the loss functions for the near user, and determine the mapping and demapping between the BS and the near user. In stage II, by fixing the DNN modules learned in stage I, we minimize the loss function for the entire network, and determine the mapping and demapping for the near and far users, respectively. Both stages involve self-supervised training, utilizing the input training data as the class labels and thereby eliminating the need for human labeling effort. Instead of adopting the conventional symbol-wise training methods [22]–[24], we propose a novel bit-wise training method to obtain bit-wise soft probability outputs, facilitating the incorporation of channel coding and soft decoding to combat signal deterioration.

Then we examine the specific probability distribution that each DNN module has learned, abandoning the “black-box of learning in DNN” [25] and offering insights into the mechanism and the rationale behind the proposed DNN architecture and its corresponding training method. Besides, we propose a solution to handle the power allocation (PA) mismatch between the training and inference processes to enhance the model adaptation. Our simulation results demonstrate that the proposed deep cooperative NOMA significantly outperforms both OMA and the conventional cooperative NOMA in terms of the BER performance. Besides, the proposed scheme features a low computational complexity in both uncoded and coded cases.

The main contributions can be summarized as follows.

- We propose a novel deep cooperative NOMA scheme with bit-wise soft probability outputs, where the entire system is re-designed by a hybrid-cascaded DNN architecture, such that it can be optimized in a holistic manner.
- By constructing multiple loss functions to quantify the BER performance, we propose a novel multi-task oriented two-stage training method to solve the end-to-end training problem in a self-supervised manner.
- We carry out theoretical analysis based on information theory to reveal the learning mechanism of each DNN module. We also adapt the proposed scheme to handle the PA mismatch between training and inference, and incorporate it with channel coding.
- Our simulation results demonstrate the superiority of the proposed scheme over OMA and the conventional cooperative NOMA in various channel scenarios.

The rest of this paper is organized as follows. In Section II, we introduce the cooperative NOMA system model and the limitations of the conventional scheme. In Section III, our deep cooperative NOMA and the multi-task learning problem is introduced, and the two-stage training method is presented, followed by the analysis of the bit-wise loss function. Section IV provides the theoretical perspective of the design principles. Section V discusses the adaptation of the proposed scheme. Simulation results are shown in Section VI. Finally, the conclusion is presented in Section VII.

*Notation:* Bold lower case letters denote vectors.  $(\cdot)^T$  and  $(\cdot)^*$  denote the transpose and conjugate operations, respectively.  $\text{diag}(\mathbf{a})$  denotes a diagonal matrix whose diagonal entries starting in the upper left corner are  $a_1, \dots, a_n$ .  $\mathbb{C}$  represents the set of complex numbers.  $\mathbb{E}[\cdot]$  denotes the expected value.  $\mathbf{x}(r)$  denotes the  $r$ -th element of  $\mathbf{x}$ . Random variables are denoted by capital font, e.g.,  $X$  with the realization  $x$ . Multivariate random variables are represented by capital bold font, e.g.,  $\mathbf{Y} = [Y_1, Y_2]^T$ ,  $\mathbf{X}(r)$ , with realizations  $\mathbf{y} = [y_1, y_2]^T$ ,  $\mathbf{x}(r)$ , respectively.  $p(x, y)$ ,  $p(y|x)$ , and  $I(X; Y)$  represent the joint probability distribution, conditional probability distribution, and mutual information of the two random variables  $X$  and  $Y$ . The cross-entropy of two discrete distributions  $p(x)$  and  $q(x)$  is denoted by  $H(p(x), q(x)) = -\sum_x p(x) \log q(x)$ .

## II. COOPERATIVE NOMA COMMUNICATION SYSTEM

### A. System Model

We consider a downlink cooperative NOMA system with a BS and two users (near user UN and far user UF), as shown in Fig. 1. The BS and users are assumed to be equipped with a single antenna.

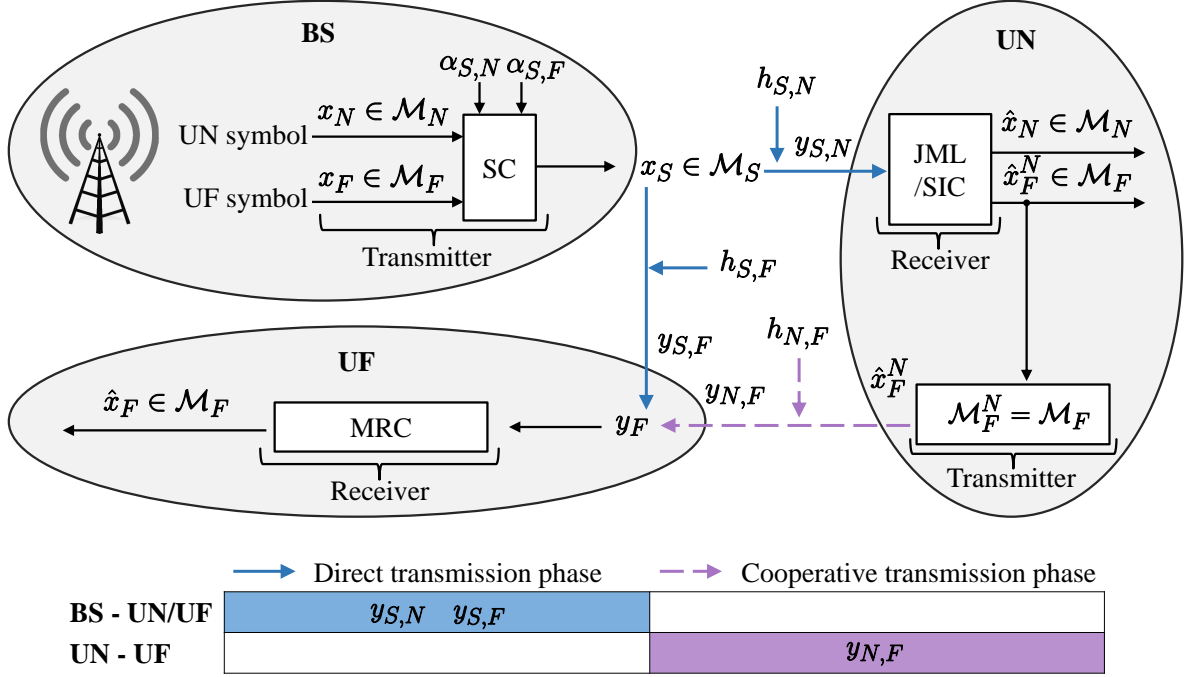


Fig. 1: System model of the cooperative NOMA. UN can adopt the JML or SIC detector.

It is considered that only the statistical channel state information (CSI), such as the average channel gains, are available at the BS, the instantaneous CSI of the BS to UN link is available at UN, and the instantaneous CSI of the BS/UN to UF links are available at UF. UN and UF are classified according to their statistical CSI. Typically, they have better and worse channel conditions, respectively. Correspondingly, UN acts as a decode-and-forward (DF) relay and assists the signal transmission to UF. The complete signal transmission consists of two phases, described as follows. In the direct transmission phase, the BS transmits the composite signal to both users. In the cooperative transmission phase, UN performs joint detection, and then forwards the re-modulated UF signal to UF.

Let  $\mathbf{s}_N \in \{0,1\}^{k_N}$  and  $\mathbf{s}_F \in \{0,1\}^{k_F}$  denote the transmitted bit blocks for UN and UF, with lengths  $k_N$  and  $k_F$ , respectively.  $\mathbf{s}_N$  and  $\mathbf{s}_F$  are mapped to user symbols  $x_N$  and  $x_F$ , taking from  $M_N$ - and  $M_F$ -ary unit-power constellations  $\mathcal{M}_N \subset \mathbb{C}$  and  $\mathcal{M}_F \subset \mathbb{C}$ , respectively, where  $2^{k_N} = M_N$  and  $2^{k_F} = M_F$ . The detailed transmission process is as follows.

In the direct transmission phase, the BS uses SC to obtain a composite symbol

$$x_S = \sqrt{\alpha_{S,N}}x_N + \sqrt{\alpha_{S,F}}x_F, \quad x_S \in \mathcal{M}_S \subset \mathbb{C} \quad (1)$$

and transmits  $x_S$  to the two users, where  $\alpha_{S,N}$  and  $\alpha_{S,F}$  are the PA coefficients with  $\alpha_{S,N} < \alpha_{S,F}$  and  $\alpha_{S,N} + \alpha_{S,F} = 1$ .  $\mathcal{M}_S$  is called the composite constellation, and can be written as the sumset

$\mathcal{M}_S = \sqrt{\alpha_{S,N}}\mathcal{M}_N + \sqrt{\alpha_{S,F}}\mathcal{M}_F \triangleq \{\sqrt{\alpha_{S,N}}t_N + \sqrt{\alpha_{S,F}}t_F : t_N \in \mathcal{M}_N, t_F \in \mathcal{M}_F\}$ . The received signal at the users can be expressed as

$$y_{S,J} = \sqrt{P_S}h_{S,J}(\sqrt{\alpha_{S,N}}x_N + \sqrt{\alpha_{S,F}}x_F) + n_{S,J}, \quad J \in \{N, F\}, \quad (2)$$

where  $P_S$  is the transmit power of the BS,  $n_{S,J} \sim \mathcal{CN}(0, 2\sigma_{S,J}^2)$  denotes the i.i.d complex AWGN, and  $h_{S,J}$  denotes the fading channel coefficient. We define the transmit signal-to-noise ratio as  $\text{SNR} = \frac{P_S}{2\sigma_{S,F}^2}$ .

After receiving  $y_{S,N}$ , UN performs JML detection<sup>1</sup> given by

$$(\hat{x}_N, \hat{x}_F^N) = \arg \min_{(x_N, x_F) \in \{\mathcal{M}_N \times \mathcal{M}_F\}} \left| y_{S,N} - \sqrt{P_S}h_{S,N}(\sqrt{\alpha_{S,N}}x_N + \sqrt{\alpha_{S,F}}x_F) \right|^2, \quad (3)$$

where  $\hat{x}_N$  denotes the estimate of  $x_N$  and  $\hat{x}_F^N$  denotes the estimate of  $x_F$  at UN. The corresponding estimated user bits  $(\hat{\mathbf{s}}_N, \hat{\mathbf{s}}_F^N) \in (\{0, 1\}^{k_N}, \{0, 1\}^{k_F})$  can be demapped from  $(\hat{x}_N, \hat{x}_F^N)$ .

In the cooperative transmission phase, UN transmits the re-modulated signal  $\hat{x}_F^N$  to UF with  $\hat{x}_F^N \in \mathcal{M}_F^N = \mathcal{M}_F$ . The received signal at UF can be written as

$$y_{N,F} = \sqrt{P_N}h_{N,F}\hat{x}_F^N + n_{N,F}, \quad (4)$$

where  $P_N$  is the transmit power of UN,  $n_{N,F} \sim \mathcal{CN}(0, 2\sigma_{N,F}^2)$  denotes the AWGN, and  $h_{N,F}$  denotes the channel fading coefficient.

The entire transmission for UF can be considered as a cooperative transmission with a DF relay, i.e., UN. As UF has the knowledge of  $h_{S,F}$  and  $h_{N,F}$ , by treating the interference term  $\sqrt{\alpha_{S,N}}x_N$  in  $y_{S,F}$  as AWGN and leveraging the widely used MRC [7], [13], [26], UF first combines  $y_{S,F}$  and  $y_{N,F}$  as

$$y_F = \beta_{S,F}y_{S,F} + \beta_{N,F}y_{N,F}, \quad (5)$$

where  $\beta_{S,F} = \frac{\sqrt{P_S\alpha_{S,F}}h_{S,F}^*}{P_S\alpha_{S,N}|h_{S,F}|^2 + 2\sigma_{S,F}^2}$  and  $\beta_{N,F} = \frac{\sqrt{P_N}h_{N,F}^*}{2\sigma_{N,F}^2}$  [13]. Then, UF detects its own symbol  $x_F$  from  $y_F$  as

$$\hat{x}_F = \arg \min_{x_F \in \mathcal{M}_F} \left| y_F - (\beta_{S,F}\sqrt{P_S\alpha_{S,F}}h_{S,F} + \beta_{N,F}\sqrt{P_N}h_{N,F})x_F \right|^2. \quad (6)$$

The corresponding estimated bits  $\hat{\mathbf{s}}_F \in \{0, 1\}^{k_F}$  can be demapped from  $\hat{x}_F$ .

Hereafter, for convenience, we denote the bit to composite symbol mappings at the BS and UN as  $f_S$  and  $f_N$ , respectively, and denote the demappings at UN and UF as  $g_N$  and  $g_F$ , respectively. They are defined as

$$f_S : (\{0, 1\}^{k_N}, \{0, 1\}^{k_F}) \rightarrow \mathcal{M}_S \subset \mathbb{C}, \quad (7)$$

$$f_N : \hat{\mathbf{s}}_F^N \rightarrow \mathcal{M}_F^N \subset \mathbb{C}, \quad (8)$$

<sup>1</sup>Here we introduce JML as an example. Note that SIC can also be used.

and

$$g_N : y_{S,N} \rightarrow (\hat{\mathbf{s}}_N, \hat{\mathbf{s}}_F^N) \in (\{0, 1\}^{k_N}, \{0, 1\}^{k_F}), \quad (9)$$

$$g_F : (y_{S,F}, y_{N,F}) \rightarrow \hat{\mathbf{s}}_F \in \{0, 1\}^{k_F}. \quad (10)$$

The average symbol error rate (SER) and BER are respectively denoted as  $\mathcal{P}_{N,e_s}$  and  $\mathcal{P}_{N,e_b}$  for UN to detect the UN signal, as  $\mathcal{P}_{F,e_s}^N$  and  $\mathcal{P}_{F,e_b}^N$  for UN to detect the UF signal, and as  $\mathcal{P}_{F,e_s}$  and  $\mathcal{P}_{F,e_b}$  at UF. They are defined as  $\mathcal{P}_{N,e_s} = \mathbb{E}_{x_N}[\Pr\{x_N \neq \hat{x}_N\}]$ ,  $\mathcal{P}_{N,e_b} = \mathbb{E}_{\mathbf{s}_N}[\Pr\{\mathbf{s}_N \neq \hat{\mathbf{s}}_N\}]$ ,  $\mathcal{P}_{F,e_s}^N = \mathbb{E}_{x_F}[\Pr\{x_F \neq \hat{x}_F^N\}]$ ,  $\mathcal{P}_{F,e_b}^N = \mathbb{E}_{\mathbf{s}_F}[\Pr\{\mathbf{s}_F \neq \hat{\mathbf{s}}_F^N\}]$ ,  $\mathcal{P}_{F,e_s} = \mathbb{E}_{x_F}[\Pr\{x_F \neq \hat{x}_F\}]$ , and  $\mathcal{P}_{F,e_b} = \mathbb{E}_{\mathbf{s}_F}[\Pr\{\mathbf{s}_F \neq \hat{\mathbf{s}}_F\}]$ . Note that SER and BER are functions of the constellation mappings (i.e.,  $f_S$  and  $f_N$ ) and demappings (i.e.,  $g_N$  and  $g_F$ ). For a given design problem, the parameters  $\{k_N, k_F, \alpha_{S,N}, \alpha_{S,F}\}$  are fixed and we let  $P_S = P_N = 1$ .

### B. Limitation

The system design above has been widely adopted in the literature [6], [7], [13], [26]. In the following, we specify its three main limitations **(L1)**-**(L3)**, which serve as the underlying motivation for a new system design in Section III.

**(L1) Bit Mapping at the BS:** From the signal detection perspective, the conventional mapping from bit to composite symbol (c.f. (7)) uses a separate mapping: first  $(\{0, 1\}^{k_N}, \{0, 1\}^{k_F}) \rightarrow (\mathcal{M}_N, \mathcal{M}_F)$ , and then  $(\mathcal{M}_N, \mathcal{M}_F) \rightarrow \mathcal{M}_S$ . Typically, we can adopt Gray mapping for  $\{0, 1\}^{k_N} \rightarrow \mathcal{M}_N$  and  $\{0, 1\}^{k_F} \rightarrow \mathcal{M}_F$ , while  $\mathcal{M}_N$  and  $\mathcal{M}_F$  are chosen from the standard constellations, e.g., QAM. Then, for designing  $f_S$  in (7), only  $(\mathcal{M}_N, \mathcal{M}_F) \rightarrow \mathcal{M}_S$  needs to be optimized as follows

$$\begin{aligned} \min_{(\mathcal{M}_N, \mathcal{M}_F) \rightarrow \mathcal{M}_S \subset \mathbb{C}} \quad & \left\{ \mathcal{P}_{N,e_s}(f_S, g_N), \mathcal{P}_{F,e_s}^N(f_S, g_N) \right\} \\ \text{subject to} \quad & \text{predefined condition,} \end{aligned} \quad (11)$$

where  $g_N$  here is the JML detector in (3),  $\mathcal{P}_{N,e_s}(f_S, g_N)$  and  $\mathcal{P}_{F,e_s}^N(f_S, g_N)$  characterize the SERs associated with (3), and for example, the predefined condition can be the constellation rotation in [27]. Clearly, this disjoint design is suboptimal, resulting in a degraded error performance. For example, in Fig. 2(a),  $x_N$  and  $x_F$  are QPSK symbols with Gray mapping. Accordingly, in Fig. 2(b),  $x_S$  is the composite symbol for  $(\alpha_{S,N}, \alpha_{S,F}) = (0.4, 0.6)$ . It can be clearly seen that at the symbol level, the composite constellation  $\mathcal{M}_S$  for  $x_S$  results in a very small minimum Euclidean distance. Furthermore, a close look at  $\mathcal{M}_S$  reveals that, at the bit level, the mapping  $(\{0, 1\}^{k_N}, \{0, 1\}^{k_F}) \rightarrow \mathcal{M}_S$  is not optimized.

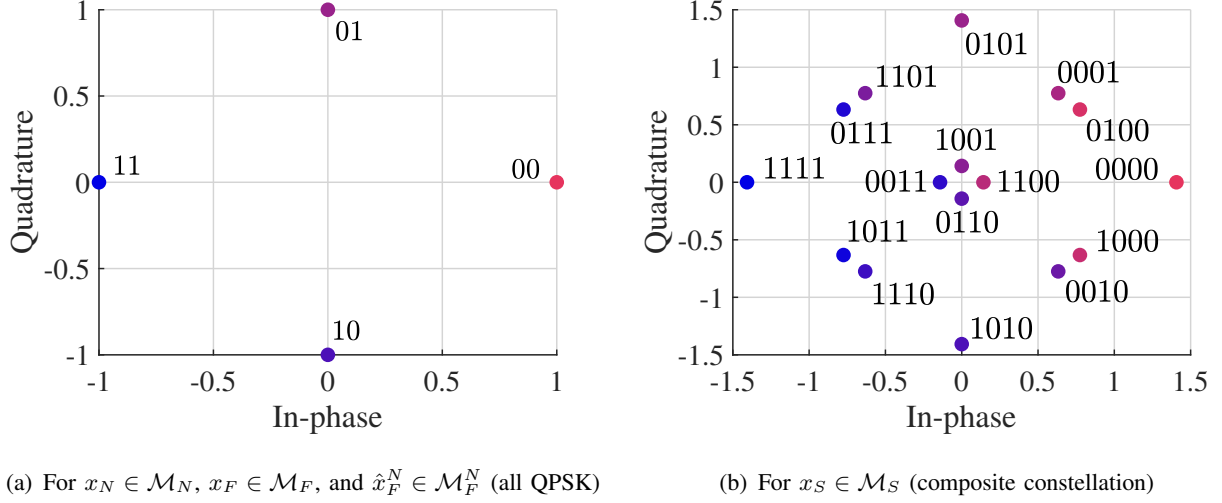


Fig. 2: Conventional constellations for  $M_N = M_F = 4$  and  $(\alpha_{S,N}, \alpha_{S,F}) = (0.4, 0.6)$ .

**(L2) Constellation at UN:** In the cooperative NOMA system, UN acts as a DF relay: first detects  $x_F$  (or equivalently,  $s_F$ ), and then forwards the re-modulated signal  $\hat{x}_F^N$  to UF. Here,  $\mathcal{M}_F^N$  is assumed in the literature to be exactly the same as the UF constellation  $\mathcal{M}_F$  at the BS. Clearly, such design for UF may not be optimal because (1) detection errors may occur at UN; (2) UF receives the signals not only from UN, but also from the BS ( $y_{S,F}$  including non-AWGN interference). In this case,  $\mathcal{M}_F^N$  should be further designed, rather than simply let  $\mathcal{M}_F^N = \mathcal{M}_F$  (known as repetition coding [28]).

**(L3) Detection at UF:** In practice, MRC is widely adopted as it only needs  $h_{S,F}$  and  $h_{N,F}$ . Its design principle can be written as

$$\begin{aligned} \min_{g_F} \quad & \mathcal{P}_{F,e_s}(f_S, f_N, g_N, g_F) \\ \text{subject to} \quad & \mathcal{M}_F^N = \mathcal{M}_F, \\ & \hat{x}_F^N = x_F, \end{aligned} \tag{12}$$

where  $\mathcal{P}_{F,e_s}(f_S, f_N, g_N, g_F)$  characterizes the SER associated with (6),  $f_S$  and  $g_N$  are given, and  $\mathcal{M}_F^N = \mathcal{M}_F$  is for  $f_N$ . However, it is sub-optimal due to the potential signal detection error at UN (i.e.,  $\hat{x}_F^N \neq x_F$ ) [11] and the ideal assumption in (6) that the interference term  $\sqrt{\alpha_{S,N}}x_N$  in  $y_{S,F}$  is AWGN.



### III. THE PROPOSED DEEP COOPERATIVE NOMA SCHEME

#### A. Motivation

To overcome **(L1)**, a desirable approach is to solve the following problem

$$\min_{f_S} \left\{ \mathcal{P}_{N,eb}(f_S, g_N), \mathcal{P}_{F,eb}^N(f_S, g_N) \right\} \quad (13)$$

with given  $g_N$ . That is, we use BER as the performance metric, and directly optimize the mapping  $f_S : (\{0, 1\}^{k_N}, \{0, 1\}^{k_F}) \rightarrow \mathcal{M}_S \subset \mathbb{C}$ . To handle **(L2)** and minimize the end-to-end BER  $\mathcal{P}_{F,eb}(f_S, f_N, g_N, g_F)$ , the constellation  $\mathcal{M}_F^N$  in  $f_N$  should be designed by solving the following problem

$$\min_{f_N} \mathcal{P}_{F,eb}(f_S, f_N, g_N, g_F) \quad (14)$$

with given  $f_S$ ,  $g_N$ , and  $g_F$ . To handle **(L3)**, the optimization problem can be re-designed as

$$\min_{g_F} \mathcal{P}_{F,eb}(f_S, f_N, g_N, g_F) \quad (15)$$

with given  $f_S$ ,  $f_N$ , and  $g_N$ , where the ideal assumptions in (12), i.e.,  $\hat{x}_F^N = x_F$  and  $\sqrt{\alpha_{S,N}}x_N$  is AWGN, are removed.

However, addressing **(L1)**-**(L3)** separately is suboptimal due to the disjoint nature of the mapping and demapping design. This motivates us to take a holistic approach, taking into account **(L1)**-**(L3)** simultaneously to perform an end-to-end multi-objective optimization as

$$\text{(P1)} \quad \min_{f_S, f_N, g_N, g_F} \left\{ \mathcal{P}_{N,eb}(f_S, g_N), \mathcal{P}_{F,eb}^N(f_S, g_N), \mathcal{P}_{F,eb}(f_S, f_N, g_N, g_F) \right\}.$$

Clearly, **(P1)** represents a joint  $\{f_S, f_N, g_N, g_F\}$  design for all objectives in (13)-(15).

**Challenge 1:** It is very challenging to find the solutions for **(P1)**, because it is difficult to transform the objective functions  $\{\mathcal{P}_{N,eb}(f_S, g_N), \mathcal{P}_{F,eb}^N(f_S, g_N), \mathcal{P}_{F,eb}(f_S, f_N, g_N, g_F)\}$  and optimization variables  $\{f_S, f_N, g_N, g_F\}$  into explicit expressions.

**Challenge 2:** Moreover, the three objectives correspond to different users' BER and may be mutually conflicting [24]. So it is very difficult to minimize them simultaneously [29].

To overcome these challenges, we propose a novel deep multi-task oriented learning scheme from a combined model- and data-driven perspective. Specifically, by tapping the strong nonlinear mapping and demapping capability of DNN (universal function approximation), we first express  $\{f_S, f_N, g_N, g_F\}$  by constructing a hybrid-cascaded DNN architecture and then transfer  $\{\mathcal{P}_{N,eb}(f_S, g_N), \mathcal{P}_{F,eb}^N(f_S, g_N), \mathcal{P}_{F,eb}(f_S, f_N, g_N, g_F)\}$  using the bit-level loss functions, so that they can be evaluated empirically. Then, we develop a multi-task oriented two-stage training method to minimize the loss functions through optimizing the DNN parameters in a self-supervised manner. Thereby the input training data also serve as the class labels.

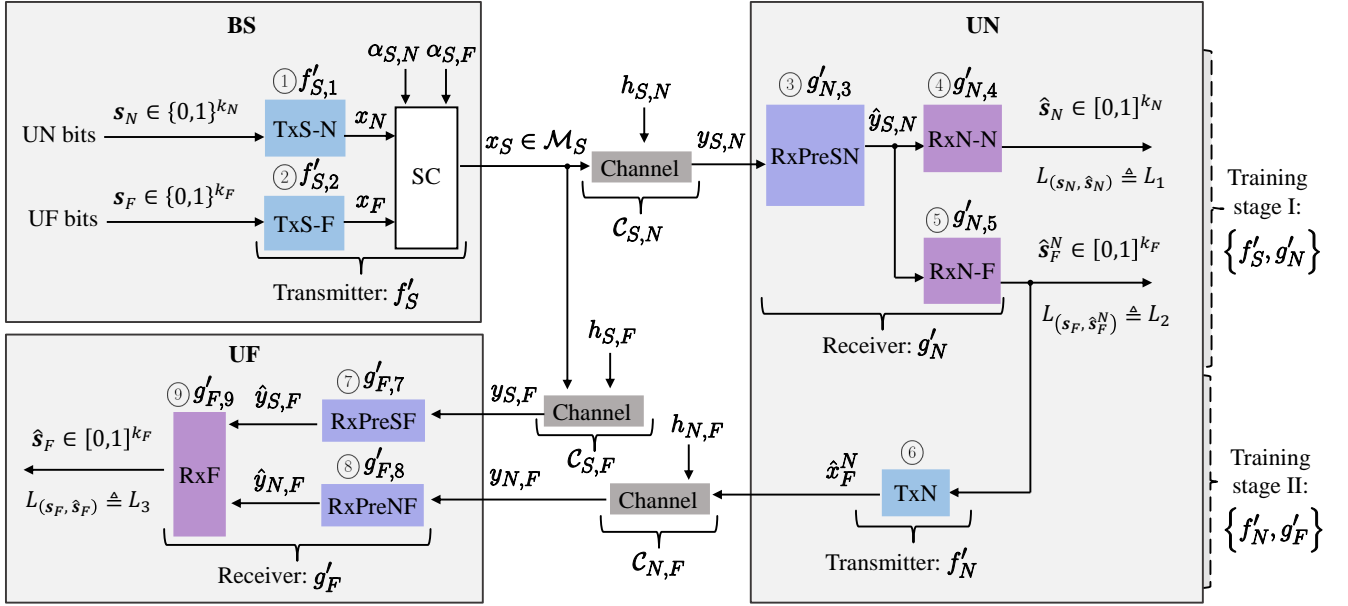


Fig. 3: Block diagram of the proposed deep cooperative NOMA including nine trainable DNN modules ①–⑨, where ①, ②, and ⑥ are mapping modules, while the remaining are demapping modules. The inputs  $\{s_N, s_F\}$  are bits, and the outputs  $\{\hat{s}_N, \hat{s}_F^N, \hat{s}_F\}$  are bit-wise soft probabilities from sigmoid function, e.g.,  $\hat{s}_F = [0.96, 0.02]$ . The corresponding loss functions are  $L_1$  and  $L_2$  for UN, and  $L_3$  for UF.

### B. Deep Cooperative NOMA

The block diagram of the proposed deep cooperative NOMA is shown in Fig. 3, where the entire system (c.f. Fig. 1) is re-designed as a novel hybrid-cascaded DNN architecture including nine trainable DNN modules, i.e., three mapping modules and six demapping modules. In essence, the whole DNN architecture learns the mapping between the BS inputs and users outputs to combat the channel fading and noise. Each DNN module consists of multiple hidden layers describing its input-output mapping, including the learnable parameters, i.e., weights and biases. Here, we adopt the offline-training and online-deploying mode in DL. This means that all the DNN modules are deployed without retraining after initial training.

At the BS, we propose to use two parallel DNN mapping modules (①TxS-N and ②TxS-F) with an SC operation to represent the direct mapping  $f_S$  in (7), which is hereafter referred to as  $f'_S : \{f'_{S,1}, f'_{S,2}\}$ , denoting the mapping parameterized by the associated DNN parameters. Note that  $f'_{S,1}$  and  $f'_{S,2}$  are for ①TxS-N and ②TxS-F, respectively. Their outputs  $x_N$  and  $x_F$  are normalized to ensure  $\mathbb{E}\{|x_N|^2\} = 1$  and  $\mathbb{E}\{|x_F|^2\} = 1$ . The composite symbol (c.f. (1)) now can be re-expressed by  $x_S = f'_S(s_N, s_F)$ . In

the direct transmission phase, the received signal at the users can be expressed as

$$y_{S,J} = h_{S,J} f'_S(\mathbf{s}_N, \mathbf{s}_F) + n_{S,J}, \quad J \in \{N, F\}. \quad (16)$$

At UN, we use three DNN demapping modules (③RxPreSN, ④RxN-N, and ⑤RxN-F) to represent the demapping in (9), referred to as  $g'_N : \{g'_{N,3}, g'_{N,4}, g'_{N,5}\}$ . Note that  $g'_{N,3}$ ,  $g'_{N,4}$ , and  $g'_{N,5}$  are for ③RxPreSN, ④RxN-N, and ⑤RxN-F, respectively. The received  $y_{S,N}$  is equalized as  $\frac{h_{S,N}^* y_{S,N}}{|h_{S,N}|^2}$ , processed by ③RxPreSN, and then demapped by two parallel DNNs (④RxN-N and ⑤RxN-F) to obtain the estimates  $\hat{\mathbf{s}}_N$  and  $\hat{\mathbf{s}}_F^N$ , respectively. This process can be expressed as

$$(\hat{\mathbf{s}}_N, \hat{\mathbf{s}}_F^N) = g'_N(y_{S,N}) \in ([0, 1]^{k_N}, [0, 1]^{k_F}), \quad (17)$$

where  $(\hat{\mathbf{s}}_N, \hat{\mathbf{s}}_F^N)$  are soft probabilities for each element in the vectors. Integrating (16)-(17), this demapping process at UN can be described as

$$\underbrace{(\hat{\mathbf{s}}_N, \hat{\mathbf{s}}_F^N)}_{(17)} = g'_N \circ \underbrace{\mathcal{C}_{S,N} \circ f'_S(\mathbf{s}_N, \mathbf{s}_F)}_{(16) \text{ with } J=N}, \quad (18)$$

where  $\circ$  is the composition operator and  $\mathcal{C}_{S,N} \triangleq \mathcal{C}_{S,N}(y_{S,N}|x_S, h_{S,N})$  denotes the channel function from the BS to UN. We refer to (18) as the first demapping phase.

After obtaining  $\hat{\mathbf{s}}_F^N$ , we use the DNN mapping module ⑥TxN to represent the mapping in (8), denoted as  $\hat{x}_F^N = f'_N(\hat{\mathbf{s}}_F^N)$ , where  $f'_N = f'_{N,6}$ . A normalization layer is used at the last layer of ⑥TxN to ensure  $\mathbb{E}\{|\hat{x}_F^N|^2\} = 1$ . In the cooperative transmission phase, UF receives

$$y_{N,F} = h_{N,F} f'_N(\hat{\mathbf{s}}_F^N) + n_{N,F}. \quad (19)$$

Finally at UF, we use three DNN demapping modules (⑦RxPreSF, ⑧RxPreNF, and ⑨RxF) to represent the demapping in (10) as  $g'_F : \{g'_{F,7}, g'_{F,8}, g'_{F,9}\}$ . Note that  $g'_{F,7}$ ,  $g'_{F,8}$ , and  $g'_{F,9}$  are for ⑦RxPreSF, ⑧RxPreNF, and ⑨RxF, respectively. The received  $y_{S,F}$  and  $y_{N,F}$  are equalized as  $\frac{h_{S,F}^* y_{S,F}}{|h_{S,F}|^2}$  and  $\frac{h_{N,F}^* y_{N,F}}{|h_{N,F}|^2}$ , processed by the parallel ⑦RxPreSF and ⑧RxPreNF, respectively, and then fed into ⑨RxF to obtain  $\hat{\mathbf{s}}_F$ . This process can be described as

$$\hat{\mathbf{s}}_F = g'_F(y_{S,F}, y_{N,F}) \in [0, 1]^{k_F}. \quad (20)$$

Note that the soft probability output  $\hat{\mathbf{s}}_F$  can serve as the input of a soft channel decoder, which will be explained in Section V-B. Integrating (16)-(20), the end-to-end demapping process at UF can be described as

$$\hat{\mathbf{s}}_F = g'_F \left( \underbrace{\mathcal{C}_{S,F} \circ f'_S(\mathbf{s}_N, \mathbf{s}_F)}_{(16) \text{ with } J=F}, \underbrace{\mathcal{C}_{N,F} \circ f'_N}_{(19)} \circ \underbrace{g'_N \circ \mathcal{C}_{S,N} \circ f'_S(\mathbf{s}_N, \mathbf{s}_F)}_{(18)} \right), \quad (21)$$

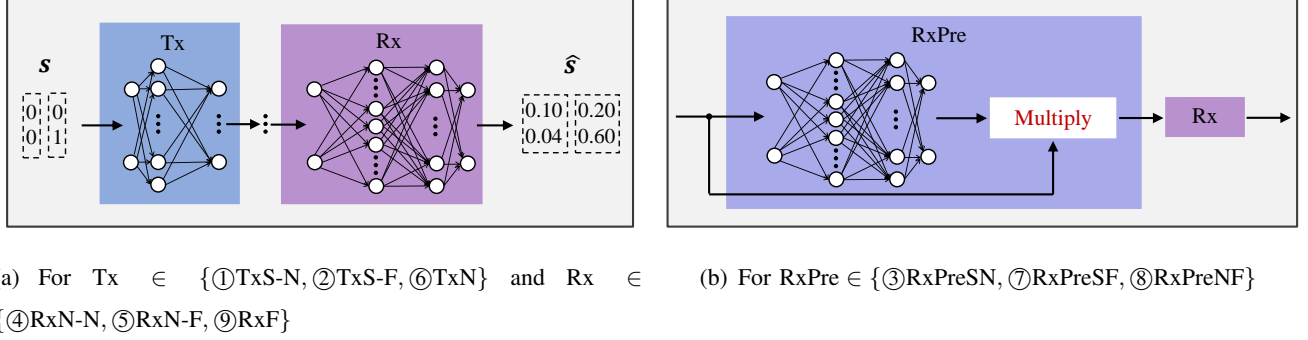


Fig. 4: Block diagram of the layer structure for the DNN modules.

where  $\mathcal{C}_{S,F} \triangleq \mathcal{C}_{S,F}(y_{S,F}|x_S, h_{S,F})$  and  $\mathcal{C}_{N,F} \triangleq \mathcal{C}_{N,F}(y_{N,F}|\hat{x}_F^N, h_{N,F})$  denote the channel functions from the BS and UN to UF, respectively. We refer to (21) as the second demapping phase.

Having presented the overall picture of the proposed DNN architecture, next we scrutinize the layer structure for each individual module. Fig. 4(a) shows the modules  $T_x \in \{\textcircled{1}TxS-N, \textcircled{2}TxS-F, \textcircled{6}TxN\}$  and  $R_x \in \{\textcircled{4}RxN-N, \textcircled{5}RxN-F, \textcircled{9}RxF\}$ , which share a common structure with multiple cascaded DNN layers. Fig. 4(b) shows the modules  $R_xPre \in \{\textcircled{3}RxPreSN, \textcircled{7}RxPreSF, \textcircled{8}RxPreNF\}$ , which share a common structure with an element-wise multiplication operation at the output layer. The main purpose of the multiplication operation is to extract the key feature for signal demapping. For example,  $\textcircled{3}RxPreSN$  is to learn the feature  $|y_{S,N} - h_{S,N}x_S|^2 = |h_{S,N}x_S|^2 - 2\text{Re}\{h_{S,N}^*x_S^*y_{S,N}\} + |y_{S,N}|^2$  containing  $|x_S|^2$ , which is key to signal demapping (c.f. (3)). The input of  $\textcircled{3}RxPreSN$  is  $\frac{h_{S,N}^*y_{S,N}}{|h_{S,N}|^2}$ . After the multiple cascaded layers learn an estimate of  $x_S$ , e.g.,  $ax_S + b$ , the element-wise multiplication operation computes  $\text{Re}\left\{\frac{h_{S,N}^*y_{S,N}}{|h_{S,N}|^2}\right\} \text{Re}\{ax_S + b\} = \text{Re}\left\{x_S + \frac{h_{S,N}^*n_{S,N}}{|h_{S,N}|^2}\right\} \text{Re}\{ax_S + b\}$  containing  $\text{Re}\{x_S\}^2$  and  $\text{Im}\left\{x_S + \frac{h_{S,N}^*n_{S,N}}{|h_{S,N}|^2}\right\} \text{Im}\{ax_S + b\}$  containing  $\text{Im}\{x_S\}^2$ .

Given the above, the DNN based joint optimization problem for the two demapping phases (18) and (21) can now be reformulated as

$$(\mathbf{P2}) \quad \min_{f'_S, f'_N, g'_N, g'_F} \left\{ L_{(s_N, \hat{s}_N)}(f'_S, g'_N), L_{(s_F, \hat{s}_F^N)}(f'_S, g'_N), L_{(s_F, \hat{s}_F)}(f'_S, f'_N, g'_N, g'_F) \right\},$$

where  $L_{(s_N, \hat{s}_N)}(f'_S, g'_N) \triangleq L_1$  denotes the loss between the input-output pair  $(s_N, \hat{s}_N)$  as a function of  $\{f'_S, g'_N\}$ , and similar definition follows for  $L_{(s_F, \hat{s}_F^N)}(f'_S, g'_N) \triangleq L_2$  and  $L_{(s_F, \hat{s}_F)}(f'_S, f'_N, g'_N, g'_F) \triangleq L_3$ . These losses measure the demapping errors for their respective input, and they will be mathematically defined in Section III-C3. Note that  $\{L_1, L_2\}$  are associated with (18), and  $L_3$  associated with (21) is the end-to-end loss for the entire network. Clearly,  $(\mathbf{P1})$  has been translated into  $(\mathbf{P2})$  in a more

tractable form, where highly nonlinear mappings and demappings are learned by training the DNN parameter set  $\{f'_S, f'_N, g'_N, g'_F\}$ . This provides a solution to **Challenge 1**.

However, we still need to address **Challenge 2**, as **(P2)** involves three loss functions. Typically, this is a multi-task learning (MTL) problem [30], which is more complex than the conventional single-task learning. Moreover, the outputs  $\{\hat{\mathbf{s}}_N, \hat{\mathbf{s}}_F^N, \hat{\mathbf{s}}_F\}$  are bit-wise probabilities for each input bit, rather than the widely used symbol-wise probabilities for each input symbol [24], [31]. Therefore, a bit-wise self-supervised training method needs to be developed and analyzed. We will address the MTL in Section III-C1, and the bit-wise self-supervised training in Sections III-C2 and III-C3.

### C. The Proposed Two-Stage Training Method

1) *Multi-Task Learning*: In this MTL problem, minimizing  $\{L_1, L_2, L_3\}$  simultaneously may lead to a poor error performance. For example, we may arrive at a situation where  $L_2$  and  $L_3$  are sufficiently small but  $L_1$  is still very large. To avoid this, we develop a novel two-stage training method by analyzing the relationship among  $\{L_1, L_2, L_3\}$ .

It is clear that  $L_1$  and  $L_2$  are related to  $\{f'_S, g'_N\}$ , while  $L_3$  is related to  $\{f'_S, f'_N, g'_N, g'_F\}$ . As  $\{f'_S, g'_N\} \subset \{f'_S, f'_N, g'_N, g'_F\}$ , this implies a causal structure between  $\{L_1, L_2\}$  and  $L_3$ . A more rigorous analysis on this relationship is provided in Appendix A. On this basis, **(P2)** can be translated into the following problem

$$\begin{aligned}
 & \text{Stage I:} && \min_{f'_S, g'_N} && \{L_1, L_2\} \\
 \text{(P3)} \quad & \text{Stage II:} && \min_{f'_N, g'_F} && L_3 \\
 & && \text{subject to} && f'_S, g'_N.
 \end{aligned}$$

For **(P3)**, as shown in Fig. 3, in stage I we minimize  $L_1$  and  $L_2$  through learning  $\{f'_S, g'_N\}$  by data training. In stage II, we minimize  $L_3$  through learning  $\{f'_N, g'_F\}$  by fixing the obtained  $\{f'_S, g'_N\}$  in stage I. It is worth noting that stage I is still a MTL problem, but we can minimize  $L_1$  and  $L_2$  simultaneously since they share the same  $\{f'_S, g'_N\}$ .

2) *Self-Supervised Training*: For convenience, we express the three loss functions  $L_1, L_2$ , and  $L_3$  in a unified form. On this basis, we elaborate on the self-supervised training method for fading channels. Without loss of generality, we let  $k_N = k_F = k$ , and  $(k, \alpha_{S,N}, \alpha_{S,F})$  are fixed during the training.

From **(P2)**,  $L_1, L_2$ , and  $L_3$  can be written as

$$L_{(s,\hat{s})}(f', g') \triangleq \mathbb{E}_s[\mathcal{L}(s, \hat{s})], \quad (s, \hat{s}) \in \{(s_N, \hat{s}_N), (s_F, \hat{s}_F), (s_F, \hat{s}_F^N)\}, \quad (22)$$

where the input bits  $\mathbf{s}$  also serve as the labels,  $\hat{\mathbf{s}}$  denotes the output soft probabilities, and  $\mathcal{L}(\mathbf{s}, \hat{\mathbf{s}})$  denotes the adopted loss function such as mean squared error and cross-entropy (CE) [14, Ch. 5]. For  $f'$  and  $g'$  specifically, we have

$$(f', g') = \begin{cases} (f'_S, g'_N), & \text{for } (\mathbf{s}, \hat{\mathbf{s}}) \in \{(\mathbf{s}_N, \hat{\mathbf{s}}_N), (\mathbf{s}_F, \hat{\mathbf{s}}_F^N)\}, \\ (\{f'_S, f'_N\}, \{g'_N, g'_F\}), & \text{for } (\mathbf{s}, \hat{\mathbf{s}}) = (\mathbf{s}_F, \hat{\mathbf{s}}_F). \end{cases} \quad (23)$$

For a random batch of training examples  $\{(\mathbf{s}^b, \hat{\mathbf{s}}^b)\}_{b=1}^B$  of size  $B$ , the loss in (22) can be estimated through sampling as

$$L_{(\mathbf{s}, \hat{\mathbf{s}})}(f', g') = \frac{1}{B} \sum_{b=1}^B \mathcal{L}(\mathbf{s}^b, \hat{\mathbf{s}}^b). \quad (24)$$

We use the stochastic gradient decent (SGD) algorithm to update the DNN parameter set  $\{f', g'\}$  through backpropagation [14, Ch. 6.5] as

$$\{f', g'\}^{(t)} = \{f', g'\}^{(t-1)} - \tau \nabla L_{(\mathbf{s}, \hat{\mathbf{s}})}(\{f', g'\}^{(t-1)}), \quad (25)$$

starting with a random initial value  $\{f', g'\}^{(0)}$ , where  $\tau > 0$ ,  $t$ , and  $\nabla$  denote the learning rate, iteration index, and gradient operator, respectively.

For the specific offline training of **(P3)**, following the proposed two-stage training method, the DNN parameter set  $\{f'_S, f'_N, g'_N, g'_F\}$  is first learned under AWGN channels ( $\mathbf{h} = [h_{S,N}, h_{S,F}, h_{N,F}]^T = [3, 1, 3]^T$ ) to combat the noise. Then, by fixing  $\{f'_S, f'_N\}$ , only  $\{g'_N, g'_F\}$  are fine-tuned under fading channels ( $\mathbf{h} \sim \mathcal{CN}(0, \mathbf{\Lambda})$  with  $\mathbf{\Lambda} = \text{diag}([\lambda_{S,N}, \lambda_{S,F}, \lambda_{N,F}]^T)$ ) to combat signal fluctuation.

Another critical issue is that, in the most literature [22], [24],  $L_{(\mathbf{s}, \hat{\mathbf{s}})}(f', g')$  only represents the symbol-level CE loss with softmax activation function [14], where  $\mathbf{s}$  is represented by a one-hot vector of length  $2^k$ , i.e., only one element equals to one and others zero [22]. Fundamentally different from [22], [24],  $L_{(\mathbf{s}, \hat{\mathbf{s}})}(f', g')$  here characterizes the bit-level loss, thereby requiring further analysis.

3) *Bit-Level Loss*: Because the inputs  $\{\mathbf{s}_N, \mathbf{s}_F\}$  are binary bits,  $L_{(\mathbf{s}, \hat{\mathbf{s}})}(f', g')$  minimization is a binary classification problem, where we use the binary cross-entropy (BCE) loss to quantify the demapping error. Accordingly, sigmoid activation function, i.e.,  $\phi(z) = \frac{1}{1+e^{-z}}$ , is used at the output layers of ④RxN-N, ⑤RxN-F, and ⑨RxF to obtain bit-wise soft probabilities  $\hat{\mathbf{s}}_N$ ,  $\hat{\mathbf{s}}_F^N$ , and  $\hat{\mathbf{s}}_F$ , respectively. In this case, following (22), the BCE loss function can be written as

$$\begin{aligned} \mathcal{L}(\mathbf{s}, \hat{\mathbf{s}}) &= \sum_{r=1}^k \mathcal{L}(\mathbf{s}(r), \hat{\mathbf{s}}(r)) \\ &= - \sum_{r=1}^k \left( \mathbf{s}(r) \log \hat{\mathbf{s}}(r) + (1 - \mathbf{s}(r)) \log(1 - \hat{\mathbf{s}}(r)) \right), \\ &(\mathbf{s}, \hat{\mathbf{s}}) \in \{(\mathbf{s}_N, \hat{\mathbf{s}}_N), (\mathbf{s}_F, \hat{\mathbf{s}}_F^N), (\mathbf{s}_F, \hat{\mathbf{s}}_F)\}. \end{aligned} \quad (26)$$

In another form,  $\mathcal{L}(\mathbf{s}, \hat{\mathbf{s}})$  can be shown as

$$\begin{aligned}\mathcal{L}(\mathbf{s}, \hat{\mathbf{s}}) &= H(p_{f'}(\mathbf{s}), \hat{p}_{g'}(\mathbf{s})) \\ &= \sum_{r=1}^k \mathbb{E}_{\mathbf{s}(r)} [H(\mathbf{s}(r), \hat{\mathbf{s}}(r))],\end{aligned}\quad (27)$$

where  $H(\cdot)$  represents the cross-entropy between the parameterized distributions  $p_{f'}(\mathbf{s})$  and  $\hat{p}_{g'}(\mathbf{s})$ .  $p_{f'}(\mathbf{s})$  denotes the true distribution of  $\mathbf{s}$  for the transmitter with  $f'$ , while  $\hat{p}_{g'}(\mathbf{s})$  denotes the estimated distribution of  $\mathbf{s}$  for the receiver with  $g'$ . We can see from (27) that the optimization is performed for each individual bits in  $\mathbf{s}$ .

Then, during training,  $L_{(\mathbf{s}, \hat{\mathbf{s}})}(f', g')$  can be computed through averaging over all possible channel outputs  $\mathbf{y} = [y_{S,N}, y_{S,F}, y_{N,F}]^T$  according to

$$\begin{aligned}L_{(\mathbf{s}, \hat{\mathbf{s}})}(f', g') &= \sum_{r=1}^k \mathbb{E}_{\mathbf{s}(r), \mathbf{y}} [H(p_{f'}(\mathbf{s}(r)|\mathbf{y}), \hat{p}_{g'}(\mathbf{s}(r)|\mathbf{y}))] \\ &= H(\mathbf{S}) - \sum_{r=1}^k I_{f'}(\mathbf{S}(r); \mathbf{Y}) + \sum_{r=1}^k \mathbb{E}_{\mathbf{y}} [D_{\text{KL}}(p_{f'}(\mathbf{s}(r)|\mathbf{y}) \parallel \hat{p}_{g'}(\mathbf{s}(r)|\mathbf{y}))],\end{aligned}\quad (28)$$

where  $I(\cdot; \cdot)$  is the mutual information (MI), and  $D_{\text{KL}}(p \parallel \hat{p})$  is the Kullback-Leibler (KL) divergence between distributions  $p$  and  $\hat{p}$  [32]. The first term on the right side of (28) is the entropy of  $\mathbf{s}$ , which is a constant. The second term can be viewed as learning  $f'$  at the transmitter, i.e.,  $(\{0, 1\}^{k_N}, \{0, 1\}^{k_F}) \rightarrow \mathcal{M}_S$  and  $\hat{\mathbf{s}}_F^N \rightarrow \mathcal{M}_F^N$ . The third term measures the difference between the true distribution  $p_{f'}(\mathbf{s}(r)|\mathbf{y})$  at the transmitter and the learned distribution  $\hat{p}_{g'}(\mathbf{s}(r)|\mathbf{y})$  at the receiver, which corresponds to  $y_{S,N} \rightarrow (\hat{\mathbf{s}}_N, \hat{\mathbf{s}}_F^N) \in (\{0, 1\}^{k_N}, \{0, 1\}^{k_F})$  and  $(y_{S,F}, y_{N,F}) \rightarrow \hat{\mathbf{s}}_F \in \{0, 1\}^{k_F}$ .

#### IV. A THEORETICAL PERSPECTIVE OF THE DESIGN PRINCIPLES

In Section III, we illustrated the whole picture of the proposed DNN architecture for deep cooperative NOMA. In this section, we further analyze the specific probability distribution that each DNN module has learned, through studying the loss functions in (28) for each training stage of **(P3)**.

##### A. Training Stage I

In essence, training stage I is MTL over a multiple access channel with inputs  $\{\mathbf{s}_N, \mathbf{s}_F\}$ , transceiver  $\{f'_S, g'_N\}$ , channel function  $\mathcal{C}_{S,N}$ , and outputs  $\{\hat{\mathbf{s}}_N, \hat{\mathbf{s}}_F^N\}$ . From information theory [32], the correspond-

ing loss functions  $L_1$  and  $L_2$  for the two tasks can be expressed as

$$\begin{aligned}
L_1 &= H(\mathbf{S}_N) - \underbrace{\sum_{r=1}^k I_{f'_S}(\mathbf{S}_N(r); Y_{S,N})}_{\text{Conflicting MI}} + \sum_{r=1}^k \mathbb{E}_{y_{S,N}} \left[ D_{\text{KL}}(p_{f'_S}(\mathbf{s}_N(r)|y_{S,N}) \parallel \hat{p}_{g'_{N,4}}(\mathbf{s}_N(r)|y_{S,N})) \right] \quad (29) \\
&= H(\mathbf{S}_N) - \underbrace{\sum_{r=1}^k I_{f'_S}(\mathbf{S}_N(r), \mathbf{S}_F(r); Y_{S,N})}_{\text{Common MI}} + \sum_{r=1}^k I_{f'_{S,2}}(\mathbf{S}_F(r); Y_{S,N} | \mathbf{S}_N(r)) + \sum_{r=1}^k \mathbb{E}_{y_{S,N}} \left[ D_{\text{KL}} \right. \\
&\quad \left. \left( \int_{x_S} \underbrace{p_{f'_S}(\mathbf{s}_N(r)|x_S)}_{\text{Individual distribution}} \underbrace{p(x_S|y_{S,N})}_{\text{Common distribution}} dx_S \parallel \int_{\hat{y}_{S,N}} \underbrace{\hat{p}_{g'_{N,4}}(\mathbf{s}_N(r)|\hat{y}_{S,N})}_{\text{Individual module}} \underbrace{\hat{p}_{g'_{N,3}}(\hat{y}_{S,N}|y_{S,N})}_{\text{Common module}} d\hat{y}_{S,N} \right) \right], \quad (30)
\end{aligned}$$

where  $\hat{y}_{S,N}$  denotes the output signal of ③RxPreSN, and the derivations for (29) and (30) are given in Appendix B.

Similarly, we have

$$\begin{aligned}
L_2 &= H(\mathbf{S}_F) - \underbrace{\sum_{r=1}^k I_{f'_S}(\mathbf{S}_N(r), \mathbf{S}_F(r); Y_{S,N})}_{\text{Common MI}} + \underbrace{\sum_{r=1}^k I_{f'_{S,1}}(\mathbf{S}_N(r); Y_{S,N} | \mathbf{S}_F(r))}_{\text{Conflicting MI}} + \sum_{r=1}^k \mathbb{E}_{y_{S,N}} \left[ D_{\text{KL}} \right. \\
&\quad \left. \left( \int_{x_S} \underbrace{p_{f'_S}(\mathbf{s}_F(r)|x_S)}_{\text{Individual distribution}} \underbrace{p(x_S|y_{S,N})}_{\text{Common distribution}} dx_S \parallel \int_{\hat{y}_{S,N}} \underbrace{\hat{p}_{g'_{N,5}}(\mathbf{s}_F(r)|\hat{y}_{S,N})}_{\text{Individual module}} \underbrace{\hat{p}_{g'_{N,3}}(\hat{y}_{S,N}|y_{S,N})}_{\text{Common module}} d\hat{y}_{S,N} \right) \right]. \quad (31)
\end{aligned}$$

Now we analyze the components of  $L_1$  and  $L_2$  in (29)-(31). Specifically, on one hand, (30) and (31) share a common MI term  $\sum_{r=1}^k I_{f'_S}(\mathbf{S}_N(r), \mathbf{S}_F(r); Y_{S,N})$ , which corresponds to the learning of  $f'_S$ . On the other hand, (29) and (31) have conflicting MI terms. That is, minimizing (29) leads to maximizing the second term  $\sum_{r=1}^k I_{f'_S}(\mathbf{S}_N(r); Y_{S,N})$ , while minimizing (31) results in minimizing the third term  $\sum_{r=1}^k I_{f'_{S,1}}(\mathbf{S}_N(r); Y_{S,N} | \mathbf{S}_F(r))$  with  $f'_{S,1} \subset f'_S$ . Clearly, these two objectives are contradictory for learning  $f'_S$ .

Next, let us observe the KL divergence terms in (30)-(31) at the receiver side. The true distributions in (30) and (31) share a common distribution term  $p(x_S|y_{S,N})$ , and individual (but related) distribution terms  $p_{f'_S}(\mathbf{s}_J(r)|x_S)$ ,  $J \in \{N, F\}$ . By exploiting this relationship, we use a common demapping module ③RxPreSN to learn the common distribution  $\hat{p}_{g'_{N,3}}(\hat{y}_{S,N}|y_{S,N})$  for  $p(x_S|y_{S,N})$ , such that  $\hat{y}_{S,N}$  learns to estimate  $x_S$ . Then, two individual demapping modules ④RxN-N and ⑤RxN-F are used to learn  $\hat{p}_{g'_{N,4}}(\mathbf{s}_N(r)|\hat{y}_{S,N})$  and  $\hat{p}_{g'_{N,5}}(\mathbf{s}_F(r)|\hat{y}_{S,N})$  for estimating  $p_{f'_S}(\mathbf{s}_N(r)|x_S)$  and  $p_{f'_S}(\mathbf{s}_F(r)|x_S)$ , respectively.



## B. Training Stage II

Training stage II is end-to-end training with fixed  $\{f'_S, g'_N\}$  learned from stage I. As such,  $L_3$  can be expressed as (c.f. (28))

$$L_3 = H(\mathbf{S}_F) - \sum_{r=1}^k I_{f'_N}(\mathbf{S}_F(r); Y_{S,F}, Y_{N,F}) + \sum_{r=1}^k \mathbb{E}_{y_{S,F}, y_{N,F}} \left[ D_{\text{KL}}(p_{f'_N}(\mathbf{s}_F(r)|y_{S,F}, y_{N,F}) \| \hat{p}_{g'_F}(\mathbf{s}_F(r)|y_{S,F}, y_{N,F})) \right]. \quad (32)$$

Minimizing  $L_3$  results in maximizing the second term  $\sum_{r=1}^k I_{f'_N}(\mathbf{S}_F(r); Y_{S,F}, Y_{N,F})$ , corresponding to optimizing  $f'_N$ . By probability factorization, the true distribution in the third term in (32) can be expressed as

$$\begin{aligned} p_{f'_N}(\mathbf{s}_F(r)|y_{S,F}, y_{N,F}) &= \int_{x_S} \int_{\hat{\mathbf{s}}_F^N} p(\mathbf{s}_F(r)|x_S, \hat{\mathbf{s}}_F^N, y_{S,F}, y_{N,F}) p(x_S|y_{S,F}) p_{f'_N}(\hat{\mathbf{s}}_F^N|y_{N,F}) d\hat{\mathbf{s}}_F^N dx_S \\ &= \int_{x_S} \int_{\hat{\mathbf{s}}_F^N} \underbrace{p(\mathbf{s}_F(r)|x_S, \hat{\mathbf{s}}_F^N)}_{\text{Learned by } \textcircled{9}} \underbrace{p(x_S|y_{S,F})}_{\text{Learned by } \textcircled{7}} \underbrace{p_{f'_N}(\hat{\mathbf{s}}_F^N|y_{N,F})}_{\text{Learned by } \textcircled{8}} d\hat{\mathbf{s}}_F^N dx_S, \end{aligned} \quad (33)$$

where  $p(\mathbf{s}_F(r)|x_S, \hat{\mathbf{s}}_F^N)p(x_S|y_{S,F})$  is determined through the stage I training. To exploit such factorization, we introduce auxiliary variables  $\hat{y}_{S,F}$  and  $\hat{y}_{N,F}$  to estimate  $x_S$  and  $\hat{\mathbf{s}}_F^N$ , respectively, and express the distribution  $\hat{p}_{g'}(\mathbf{s}_F(r)|y_{S,F}, y_{N,F})$  in (32) as

$$\begin{aligned} \hat{p}_{g'}(\mathbf{s}_F(r)|y_{S,F}, y_{N,F}) &= \int_{\hat{y}_{S,F}} \int_{\hat{y}_{N,F}} \hat{p}_{g'_{F,9}}(\mathbf{s}_F(r)|\hat{y}_{S,F}, \hat{y}_{N,F}) \hat{p}_{g'_{F,7}}(\hat{y}_{S,F}|y_{S,F}) \hat{p}_{g'_{F,8}}(\hat{y}_{N,F}|y_{N,F}) \\ &\quad d\hat{y}_{N,F} d\hat{y}_{S,F}, \end{aligned} \quad (34)$$

where  $\hat{y}_{S,F}$  and  $\hat{y}_{N,F}$  denote the outputs of demapping modules  $\textcircled{7}$ RxPreSF and  $\textcircled{8}$ RxPreNF, respectively. Correspondingly,  $\hat{p}_{g'_{F,7}}(\hat{y}_{S,F}|y_{S,F})$  and  $\hat{p}_{g'_{F,8}}(\hat{y}_{N,F}|y_{N,F})$  describe the learned distributions for these two modules. It can be observed that  $\hat{p}_{g'_{F,7}}(\hat{y}_{S,F}|y_{S,F})$  and  $\hat{p}_{g'_{F,8}}(\hat{y}_{N,F}|y_{N,F})$  can estimate the true distributions  $p(x_S|y_{S,F})$  and  $p_{f'_N}(\hat{\mathbf{s}}_F^N|y_{N,F})$ , respectively. Table I summarizes the distributions that the DNN demapping modules have learned. In Section VI, we will show that the learned distribution is consistent with the true one.

## V. MODEL ADAPTATION

In this section, we adapt the proposed DNN scheme to suit more practical scenarios. We first address the PA mismatch between training and inference. Then, we investigate the incorporation of the widely adopted channel coding into our proposed scheme. In both scenarios, our adaptation enjoys the benefit of reusing the original trained DNN modules without carrying out a new training process.

TABLE I: Learned distributions by the DNN demapping modules and the corresponding true ones

Demapping Module	Learned Distribution	True Distribution
③RxPreSN	$\hat{p}_{g'_{N,3}}(\hat{y}_{S,N} y_{S,N})$	$p(x_S y_{S,N})$
④RxN-N	$\hat{p}_{g'_{N,4}}(\mathbf{s}_N \hat{y}_{S,N})$	$p_{f'_S}(\mathbf{s}_N x_S)$
⑤RxN-F	$\hat{p}_{g'_{N,5}}(\mathbf{s}_F \hat{y}_{S,N})$	$p_{f'_S}(\mathbf{s}_F x_S)$
⑦RxPreSF	$\hat{p}_{g'_{F,7}}(\hat{y}_{S,F} y_{S,F})$	$p(x_S y_{S,F})$
⑧RxPreNF	$\hat{p}_{g'_{F,8}}(\hat{y}_{N,F} y_{N,F})$	$p_{f'_N}(\hat{\mathbf{s}}_F^N y_{N,F})$
⑨RxF	$\hat{p}_{g'_{F,9}}(\mathbf{s}_F \hat{y}_{S,F}, \hat{y}_{N,F})$	$p(\mathbf{s}_F x_S, \hat{\mathbf{s}}_F^N)$

### A. Adaptation to Power Allocation

In Section III, the PA coefficients  $(\alpha_{S,N}, \alpha_{S,F})$  at the BS are fixed during the training process. However, their values might change during the inference process due to the nonlinear behaviors of the power amplifier in different power regions [33], [34], resulting in the mismatch between the two processes. Denote the new PA coefficient for inference as  $\hat{\alpha}_{S,N}$  for UN, and  $\hat{\alpha}_{S,F}$  for UF.

As a solution, we propose to scale the received signals for  $g'_N$  and  $g'_F$ . The goal is to ensure that their input signal-to-interference-plus-noise ratios (SINRs) are equal to those during the inference process, i.e.,  $\frac{\hat{\alpha}_{S,N}|h_{S,N}|^2}{\hat{\alpha}_{S,F}|h_{S,N}|^2+2\sigma_{S,N}^2}$  for  $\mathbf{s}_N$  demapping by  $g'_N$ ,  $\frac{\hat{\alpha}_{S,F}|h_{S,N}|^2}{\hat{\alpha}_{S,N}|h_{S,N}|^2+2\sigma_{S,N}^2}$  for  $\mathbf{s}_F$  demapping by  $g'_N$ , and  $\frac{\hat{\alpha}_{S,F}|h_{S,F}|^2}{\hat{\alpha}_{S,N}|h_{S,F}|^2+2\sigma_{S,F}^2}$  for  $\mathbf{s}_F$  demapping by  $g'_{F,7} \subset g'_F$ . In this case, their new expressions are given by

$$\hat{\mathbf{s}}_N = g'_N \left( \frac{1}{\omega_N} y_{S,N} \right), \quad (35)$$

$$\hat{\mathbf{s}}_F^N = g'_N \left( \frac{1}{\omega_F} y_{S,N} \right), \quad (36)$$

$$\hat{\mathbf{s}}_F = g'_F \left( \frac{1}{\omega_F} y_{S,F}, y_{N,F} \right), \quad (37)$$

where the scaling factors are defined as

$$\omega_N = \sqrt{\frac{\hat{\alpha}_{S,N}}{\alpha_{S,N}}}, \quad \omega_F = \sqrt{\frac{\hat{\alpha}_{S,F}}{\alpha_{S,F}}}. \quad (38)$$

Note that in (35) and (36), given two different inputs,  $g'_N(\cdot)$  is used twice to obtain  $\hat{\mathbf{s}}_N$  and  $\hat{\mathbf{s}}_F^N$ , respectively. We prove in Appendix C that the SINR is exactly  $\frac{\hat{\alpha}_{S,N}|h_{S,N}|^2}{\hat{\alpha}_{S,F}|h_{S,N}|^2+2\sigma_{S,N}^2}$  for  $\frac{1}{\omega_N} y_{S,N}$  in (35),  $\frac{\hat{\alpha}_{S,F}|h_{S,N}|^2}{\hat{\alpha}_{S,N}|h_{S,N}|^2+2\sigma_{S,N}^2}$  for  $\frac{1}{\omega_F} y_{S,N}$  in (36), and  $\frac{\hat{\alpha}_{S,F}|h_{S,F}|^2}{\hat{\alpha}_{S,N}|h_{S,F}|^2+2\sigma_{S,F}^2}$  for  $\frac{1}{\omega_F} y_{S,F}$  in (37).

### B. Incorporation of Channel Coding

Channel coding has been widely adopted to improve the communication reliability [35]. However, the conventional DNN based symbol-wise demapping [22], [24] cannot be directly connected to a

soft channel decoder [36], [37], such as the soft low-density parity-check code (LDPC) decoder [38] and polar code decoder [39]. By contrast, our proposed scheme in Section III outputs bit-wise soft information (c.f. (18), (21)), enabling the straightforward cascade of a soft channel decoder.

Specifically, denote the information bit blocks for UN and UF as  $\mathbf{c}_N$  and  $\mathbf{c}_F$ , respectively. They are encoded as binary codewords  $\langle \mathbf{s}_N \rangle = \mathcal{E}(\mathbf{c}_N)$  and  $\langle \mathbf{s}_F \rangle = \mathcal{E}(\mathbf{c}_F)$  by channel encoder  $\mathcal{E}(\cdot)$ , and then split into multiple transmitted bit blocks (i.e.,  $\mathbf{s}_N$  and  $\mathbf{s}_F$ ), which are sent into  $f'_S$ . At the receiver, the log-likelihood ratios (LLRs) of bits in  $\mathbf{s}$  are calculated as

$$\text{LLR}(\mathbf{s}(r)) = \log \left( \frac{1 - \hat{\mathbf{s}}(r)}{\hat{\mathbf{s}}(r)} \right), \quad r \in \{1, 2, \dots, k\}, \quad (39)$$

where we interpret  $\hat{\mathbf{s}}(r)$  as the soft probability for bit  $\mathbf{s}(r)$  with  $\hat{\mathbf{s}}(r) = \Pr\{\mathbf{s}(r) = 1 | \hat{\mathbf{s}}\}$  [40]. The LLRs serve as the input of the soft channel decoder, denoted as  $\mathcal{D}(\cdot)$ .

At UN, we assume that it decodes its own information  $\mathbf{c}_N$  as  $\hat{\mathbf{c}}_N = \mathcal{D}(\text{LLR}(\langle \hat{\mathbf{s}}_N \rangle))$ , but still performs  $\hat{x}_F^N = f'_N(\hat{\mathbf{s}}_F^N)$  as in the uncoded case without decoding  $\mathbf{c}_F$  (called demapping-and-forward). These two operations are separable because we use two parallel DNNs, i.e., ④RxN-N and ⑤RxN-F, to obtain  $\hat{\mathbf{s}}_N$  and  $\hat{\mathbf{s}}_F^N$ , respectively. Note that this parallel demapping can also reduce the error propagation compared to SIC. At UF, it decodes  $\mathbf{c}_F$  as  $\hat{\mathbf{c}}_F = \mathcal{D}(\text{LLR}(\langle \hat{\mathbf{s}}_F \rangle))$ . By contrast, the conventional SIC and JML decoding schemes need to decode  $\hat{\mathbf{s}}_N$  and  $\hat{\mathbf{s}}_F^N$  jointly.

## VI. SIMULATION RESULTS

In this section, we perform simulation to verify the superiority of the proposed deep cooperative NOMA scheme, and compare it with OMA and the conventional cooperative NOMA scheme. In OMA, the BS transmits  $x_N$  and  $x_F$  to UN and UF, respectively, in two consecutive time slots, and there is no cooperation between UN and UF. Default parameters for simulation are:  $k = 2$  ( $M_N = M_F = 4$ ) and  $\sigma_{S,F} = \sigma_{S,N} = \sigma_{N,F} = \sigma$ ,  $\lambda_{S,F} = 1$ ,  $\lambda_{S,N} = \lambda_{N,F}$  for the three links. We consider six scenarios (S1-S6), and their parameters are summarized in Table II, where ‘‘cooperative link’’ refers to the BS to UN to UF link. Note that for S1-S4, we have  $(\hat{\alpha}_{S,N}, \hat{\alpha}_{S,F}) = (\alpha_{S,N}, \alpha_{S,F})$ .

For the specific layer structure of each DNN module in Fig. 3, all three transmitters (①, ② and ⑥) have the same layer structure, with an input layer (dimension of  $k_N$  or  $k_F$ ) followed by 4 hidden layers with 16, 8, 4, and 2 neurons, respectively. Modules ③, ⑦ and ⑧ also have the same layer structure. There are three hidden layers of dimensions 64, 32 and 2, respectively. Modules ④, ⑤, and ⑨ have three hidden layers of dimensions 128, 64 and 32, respectively, with output of dimension  $k_N$  or  $k_F$ . We adopt tanh as the activation function for the hidden layers [41].

TABLE II: Parameters for scenarios S1-S6

Scenario	$\lambda_{S,N}$	$(\alpha_{S,N}, \alpha_{S,F})$	Explanation
S1	10	(0.4, 0.6)	Balanced PA
S2	10	(0.25, 0.75)	Optimized PA
S3	6	(0.25, 0.75)	Weaker cooperative link
S4	6	(0.1, 0.9)	Unbalanced PA
S5	10	(0.25, 0.75)	PA mismatch: $(\hat{\alpha}_{S,N}, \hat{\alpha}_{S,F}) = (0.3, 0.7)$
S6	10	(0.25, 0.75)	PA mismatch: $(\hat{\alpha}_{S,N}, \hat{\alpha}_{S,F}) = (0.2, 0.8)$

We use Keras with TensorFlow backend to implement the proposed DNN architecture, which is first trained under AWGN channels at SNR= 5 dB, and then  $\{g'_N, g'_F\}$  are fine-tuned under Rayleigh fading channels (c.f. Section III-C2) at a list of SNR values in [15, 5, 6, 7, 30] dB to achieve a favorable error performance in both low and high SNR regions. We have the learning rate  $\tau = 0.001$  and 0.01 for AWGN and Rayleigh fading channels, respectively. After training, we test the DNN scheme for various SNRs, including those beyond the trained SNRs. In the uncoded case, the demapping rule for bit  $\mathbf{s}(r)$  is  $\text{LLR}(\mathbf{s}(r)) = \log\left(\frac{1-\hat{\mathbf{s}}(r)}{\hat{\mathbf{s}}(r)}\right) \underset{\mathbf{s}(r)=1}{\overset{\mathbf{s}(r)=0}{\geq}} 0$ .

#### A. Network Losses $L_1$ , $L_2$ , and $L_3$ during Testing

Upon obtaining the proposed DNN through training, in Fig. 5, we check whether all the losses  $L_1$ ,  $L_2$ , and  $L_3$  can be significantly reduced by our proposed two-stage training method in Section III-C. For each SNR value,  $8 \times 10^5$  data bits are randomly generated for each user, divided into  $B_t = 4 \times 10^5$  data blocks with  $k = 2$  bits per block, and then sent into the DNN. We calculate  $L_1$ ,  $L_2$ , and  $L_3$  according to (24), as well as the average loss  $\sum_{t=1}^3 L_t/3$ .

We can see that for all scenarios in Fig. 5, as SNR increases,  $L_1$ ,  $L_2$  and  $L_3$  each asymptotically decreases to a small value, e.g., 0.13 for  $L_2$  in Fig. 5(a). The only exception is that  $L_1$  in S4 (Fig. 5(d)) asymptotically decreases to 0.25, because of the relatively small PA coefficient  $\alpha_{S,N} = 0.1$ . Besides,  $L_1$ ,  $L_2$ , and  $L_3$  are all close to the average loss  $\sum_{t=1}^3 L_t/3$  within 0.14. These results indicate that the proposed two-stage training can significantly reduce  $L_1$ ,  $L_2$ , and  $L_3$ , and provide a solution to the original MTL problem (**P2**).

#### B. Learned Mappings by DNN Mapping Modules

As discussed in Section III-B, the proposed DNN can learn mappings  $(\{0, 1\}^{k_N}, \{0, 1\}^{k_F}) \rightarrow \mathcal{M}_S$  and  $\hat{\mathbf{s}}_F^N \rightarrow \mathcal{M}_F^N$  automatically, resulting in a new constellation and bit mapping. Fig. 6 presents the

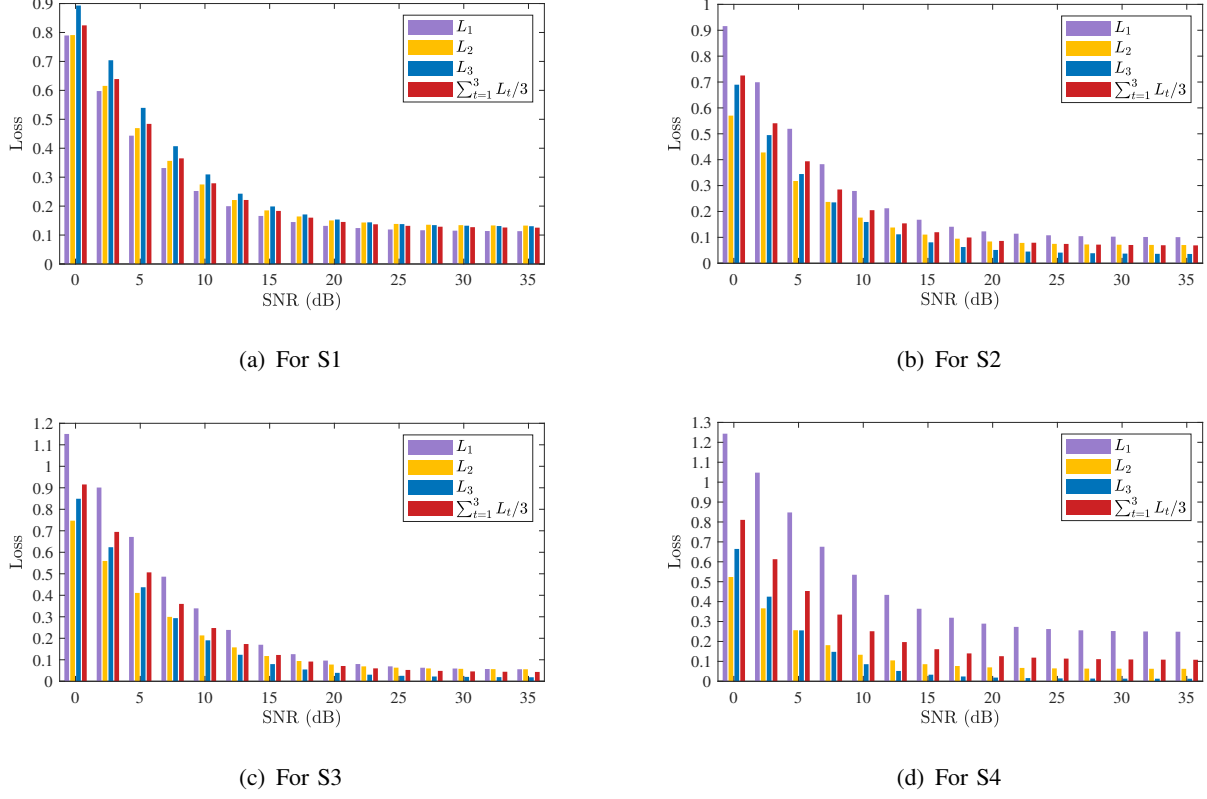
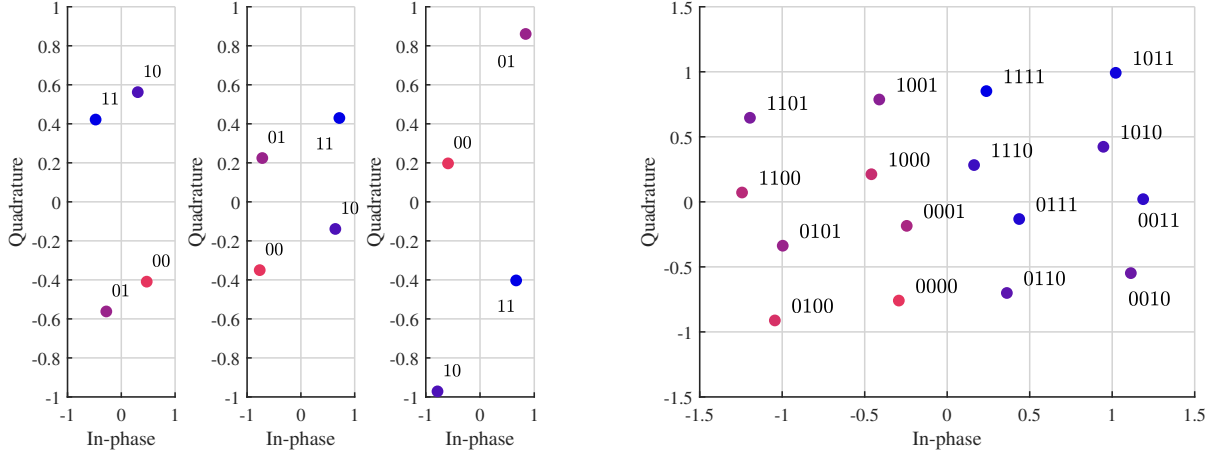


Fig. 5: Network losses  $L_1$ ,  $L_2$ ,  $L_3$ , and the average loss  $\sum_{t=1}^3 L_t/3$  for different channel scenarios.



(a) For  $\mathbf{s}_N \in \mathcal{M}_N$ ,  $\mathbf{s}_F \in \mathcal{M}_F$ , and  $\hat{\mathbf{s}}_F^N \in \mathcal{M}_F^N$ , respectively

(b) For  $\mathbf{s}_S \in \mathcal{M}_S$  (composite constellation)

Fig. 6: Learned constellations by  $f'_S$  and  $f'_N$  with bit mapping for  $(\alpha_{S,N}, \alpha_{S,F}) = (0.4, 0.6)$ .

learned constellations by  $f'_S$  and  $f'_N$  with bit mapping for  $(\alpha_{S,N}, \alpha_{S,F}) = (0.4, 0.6)$ . Fig. 6(a) shows

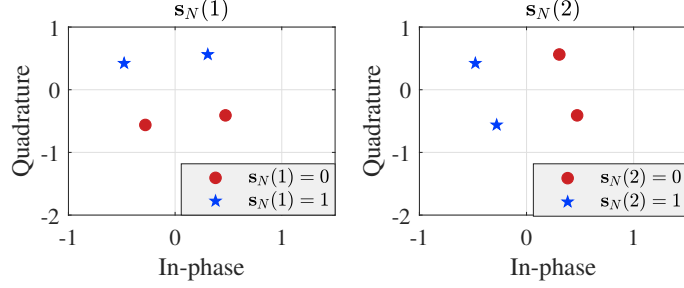
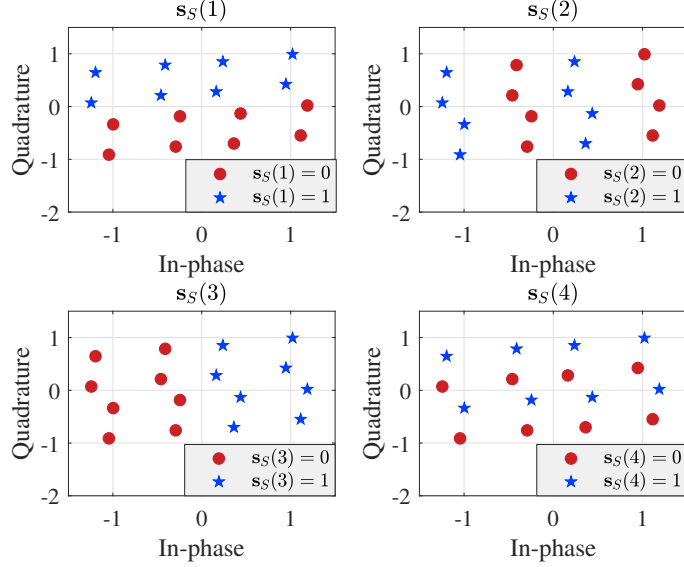
(a) For  $\mathbf{s}_N \in \mathcal{M}_N$ (b) For  $\mathbf{s}_S \in \mathcal{M}_S$  (composite constellation)

Fig. 7: Learned constellations by  $f'_S$  for the individual bit positions, where  $(\alpha_{S,N}, \alpha_{S,F}) = (0.4, 0.6)$ , and the red and blue markers denote bit 0 and 1, respectively.

the individual constellations  $\mathbf{s}_N \in \mathcal{M}_N$ ,  $\mathbf{s}_F \in \mathcal{M}_F$ , and  $\hat{\mathbf{s}}_F^N \in \mathcal{M}_F^N$ , and it can be seen that  $\mathcal{M}_N$ ,  $\mathcal{M}_F$ , and  $\mathcal{M}_F^N$  all have learned parallelogram-like shapes with different orientations and aspect ratios. Fig. 6(b) shows the composite constellation  $\mathcal{M}_S$ , where the minimum Euclidean distance is improved significantly compared with that in Fig. 2(b), i.e., from 0.2 to 0.36.

In Section III, we use the bit-wise binary classification method to achieve the demappings  $g'_N$  and  $g'_F$ . In Fig. 7, we demonstrate that the two classes (bit 0 and 1) are separable by presenting the location of each individual bit. Specifically, the constellations  $\mathbf{s}_N \in \mathcal{M}_N$  and  $\mathbf{s}_S \in \mathcal{M}_S$  in Fig. 6 are presented here in a different form in Figs. 7(a) and 7(b), respectively. It is clearly shown that these two classes (bit 0 and 1) are easily separable for all bit positions. This indicates that the demapping can be achieved.

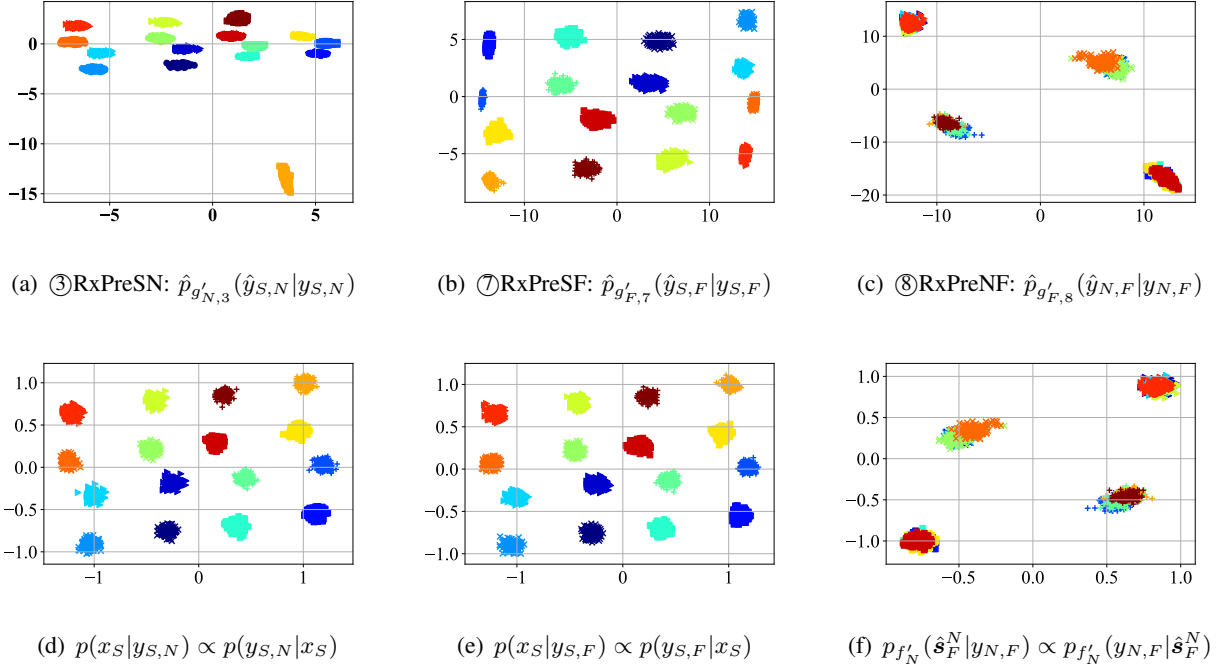
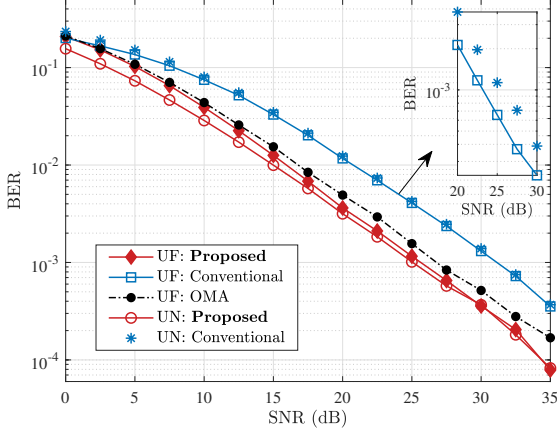


Fig. 8: Signal clusters corresponding to the learned distributions for  $\textcircled{3}\text{RxPreSN}$ ,  $\textcircled{7}\text{RxPreSF}$ , and  $\textcircled{8}\text{RxPreNF}$  (top), and the respective true ones, where  $(\alpha_{S,N}, \alpha_{S,F}) = (0.4, 0.6)$ ,  $\mathbf{h} = [1, 1, 1]^T$ , and  $\text{SNR} = 25$  dB. The x-axis and y-axis denote the in-phase and quadrature parts, respectively.

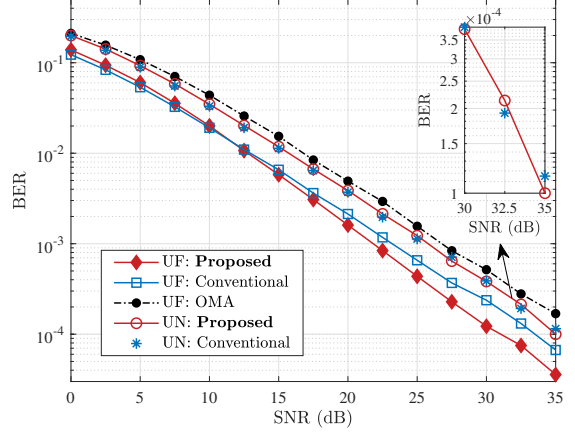
### C. Learned Distributions by DNN Demapping Modules

The learned distributions of  $\textcircled{3}\text{RxPreSN}$ ,  $\textcircled{7}\text{RxPreSF}$ , and  $\textcircled{8}\text{RxPreNF}$  for demapping and the corresponding true ones are shown in Table I. Here, to verify that  $\textcircled{3}$ ,  $\textcircled{7}$ , and  $\textcircled{8}$  have successfully learned their respective true distributions, we visualize these distributions in Fig. 8 by sampling, where each colored cluster consists of 200 signal points. The results for  $\textcircled{3}$ ,  $\textcircled{7}$ , and  $\textcircled{8}$  are shown in Figs. 8(a), 8(b), and 8(c), respectively, while the corresponding true distributions in Figs. 8(d), 8(e), and 8(f), respectively.

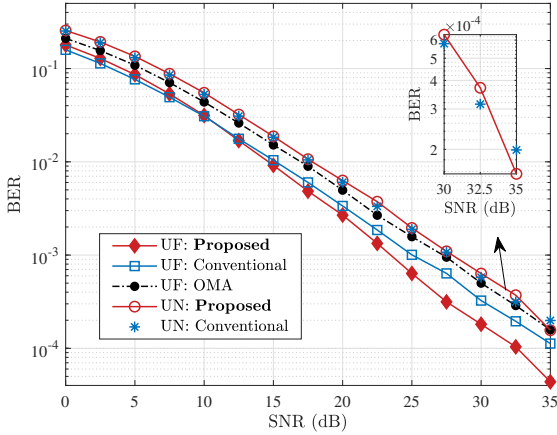
It is shown that the two figures in the same column have similar cluster shapes, indicating that  $\textcircled{3}$ ,  $\textcircled{7}$ , and  $\textcircled{8}$  have successfully learned the true distributions. Besides, it can be seen that various forms of signal transformations have been learned. For example, Fig. 8(a) can be regarded as a non-uniformly scaled version of Fig. 8(d), Fig. 8(b) can be regarded as a rotated and scaled version of Fig. 8(e), while Fig. 8(c) can be regarded as a mirrored and scaled version of Fig. 8(f). These transformations keep the original signal structure, and meanwhile can introduce more degrees of freedom to facilitate demapping. Similar observations are made in other scenarios.



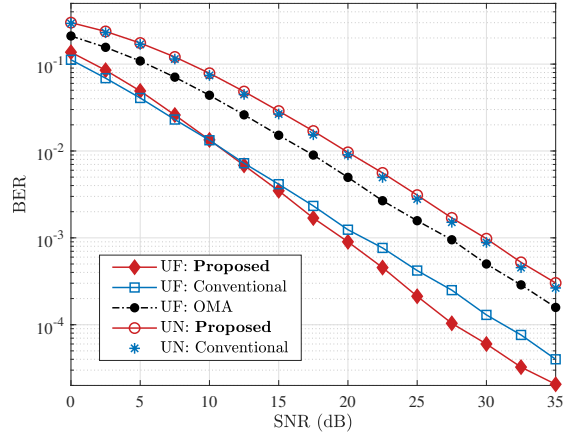
(a) For S1



(b) For S2



(c) For S3



(d) For S4

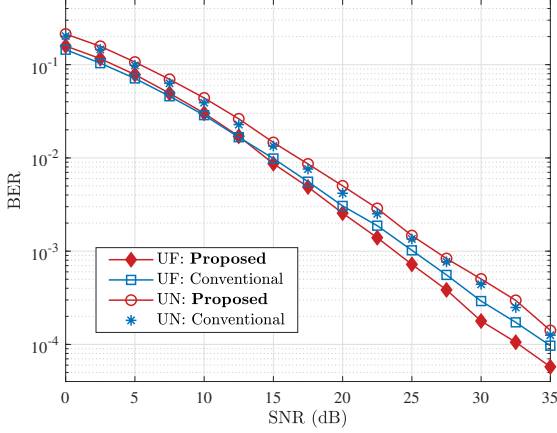
Fig. 9: BER performance comparison of the proposed deep cooperative NOMA scheme, OMA, and the conventional NOMA scheme for different channel scenarios.

#### D. Uncoded BER Performance Comparison for S1-S4

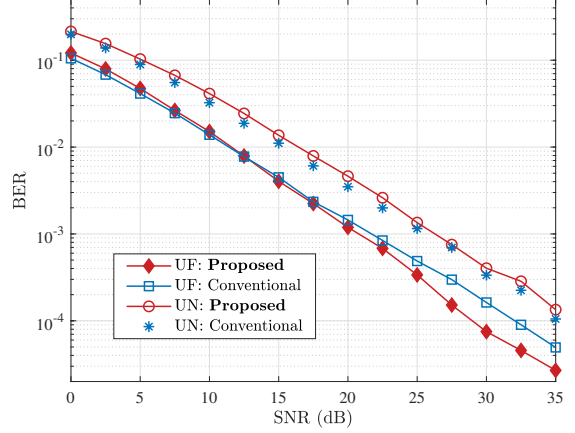
Fig. 9 compares the uncoded BER performance of the proposed deep cooperative NOMA, OMA, and the conventional NOMA for  $(\alpha_{S,N}, \alpha_{S,F}) = (\hat{\alpha}_{S,N}, \hat{\alpha}_{S,F})$ , i.e., the PA coefficients for training and inference are the same.

We first consider the scenario S1 in Fig. 9(a). It is clearly shown that the proposed scheme significantly outperforms the conventional one by 6.25 dB for both UN and UF, while outperforming the OMA by 1.25 dB at  $\text{BER}=10^{-3}$ . It can also be seen that the conventional scheme is worse than the OMA scheme in S1, due to the lack of an appropriate PA.





(a) For S5



(b) For S6

Fig. 10: BER performance comparison of the proposed deep cooperative NOMA and the conventional NOMA schemes with PA mismatch between training and inference.

We then compare the BER with optimized PA coefficients  $(\alpha_{S,N}, \alpha_{S,F})$ , as shown in Fig. 9(b) for S2. We can see that for UF, the proposed scheme outperforms the conventional one when  $\text{SNR} \geq 12.5$  dB, while outperforming the OMA across the whole SNR range. For example, the performance gap between the proposed scheme and the conventional one (resp. OMA) is around 2.5 dB (resp. 5 dB) at  $\text{BER}=10^{-4}$  (resp.  $10^{-3}$ ). For UN, the proposed scheme has a similar BER performance with the conventional one. Together with Fig. 9(a), we can see that the proposed scheme is robust to the PA.

In Fig. 9(c), we compare the BER in S3 with channel conditions different from S1 and S2. Likewise, for UF, the proposed scheme outperforms the conventional one for  $\text{SNR} > 12.5$  dB, e.g., by 3 dB at  $\text{BER}=10^{-4}$ . It outperforms the OMA across the whole SNR range, e.g., by 3 dB at  $\text{BER}=10^{-4}$ . Fig. 9(d) compares the BER in S4 with an unbalanced PA, i.e.,  $(\alpha_{S,N}, \alpha_{S,F}) = (0.1, 0.9)$ . Similar observations to Fig. 9(c) can be made, and the proposed scheme outperforms both OMA and the conventional one. Moreover, we can see from Figs. 9(b)-9(d) that the proposed scheme shows a larger decay rate for UF BER for large SNRs, revealing that the demapping errors at UN are successfully learned and compensated at UF, achieving higher diversity orders.

### E. Adaptation to Power Allocation for S5 and S6

To demonstrate its adaptation to the mismatch between the training and inference PA discussed in Section V-A, we validate the proposed scheme in S5 ( $\hat{\alpha}_{S,F} < \alpha_{S,F}$ ) and S6 ( $\hat{\alpha}_{S,F} > \alpha_{S,F}$ ) in Figs. 10(a) and 10(b), respectively. It can be seen that for UF, the proposed scheme outperforms the conventional

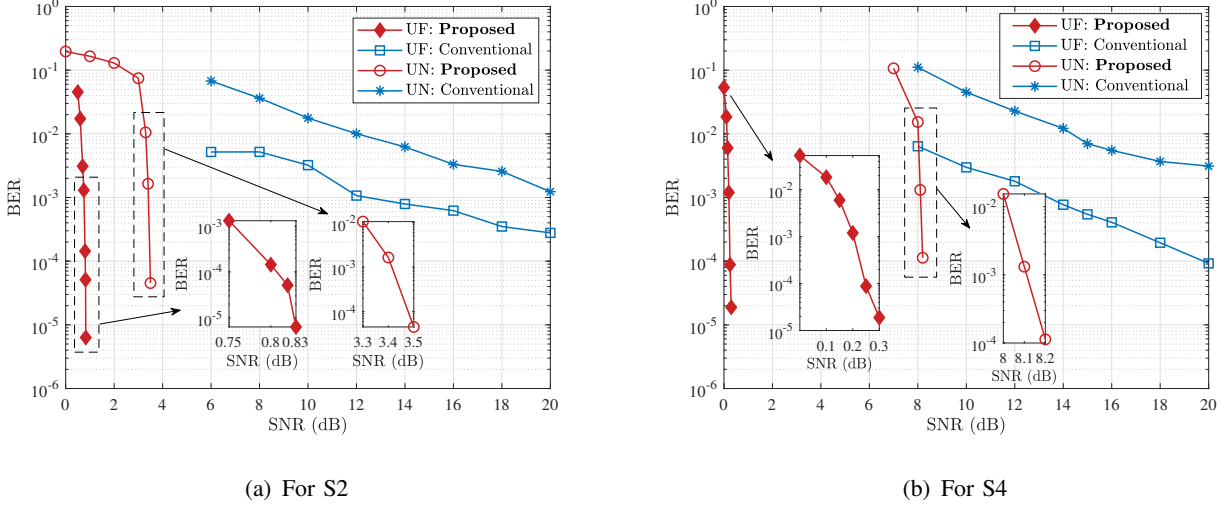


Fig. 11: BER performance comparison of the proposed deep cooperative NOMA and the conventional NOMA schemes with the LDPC code.

one at  $\text{SNR} > 15$  dB. It can also be seen that the proposed scheme still achieves larger BER decay rates in both S5 and S6. These results clearly verify that, without carrying out a new training process, the proposed scheme can handle the PA mismatch.

#### F. BER Performance Comparison with Channel Coding

In Fig. 11, we evaluate the coded BER performance with the LDPC code in S2 and S4. The code parity-check matrix comes from the DVB-S2 standard [42] with the rate  $1/2$  and size of  $32400 \times 64800$ . Therefore,  $\mathbf{c}_N$  and  $\mathbf{c}_F$  have the length of 32400 bits, while the  $\mathcal{E}(\cdot)$  encoded  $\langle \mathbf{s}_N \rangle$  and  $\langle \mathbf{s}_F \rangle$  have the length of 64800 bits. The LDPC decoder  $\mathcal{D}(\cdot)$  is based on the classic belief propagation algorithm with soft LLR as input. The coded BER is defined as  $\Pr\{\mathbf{c}_J \neq \hat{\mathbf{c}}_J\}$ ,  $J \in \{N, F\}$ . For the conventional scheme, UN adopts SIC due to its low computational complexity. Specifically, it first decodes  $\mathbf{c}_F$  as  $\hat{\mathbf{c}}_F^N = \mathcal{D}(\cdot)$ , cancels the interference after re-encoding and re-modulating  $\hat{\mathbf{c}}_F^N$ , and then decodes  $\hat{\mathbf{c}}_N$ . Then, UN forwards the re-modulated signal to UF. Note that the decoding is terminated on reaching the maximum number of decoding iterations (50 here) or when all parity checks are satisfied.

In both scenarios, we observe a significant increasing decoding performance gap between the proposed and conventional schemes. For example, in Fig. 11(b), to achieve  $\text{BER}=10^{-4}$  for UF, the SNRs for the proposed and the conventional<sup>2</sup> schemes are 0.25 and 20 dB, respectively, which shows a

<sup>2</sup>The performance of the conventional scheme can also be found in [38].

gap more than 19 dB. Similar observations can be made from Fig. 11(a). The performance superiority of the proposed scheme mainly originates from its utilizations of soft information and the parallel demapping at UN attributing to the error performance optimization. In the meantime, the performance of the conventional scheme is limited to the interference and error propagation [38].

### G. Computational Complexity Comparisons

As discussed before, we adopt the offline-training and online-deploying mode for the proposed scheme. Therefore, we only need to consider the computational complexity in the online-deploying phase. Specifically, in the uncoded case, the complexity for signal detection is  $\mathcal{O}(2^k)$  for the conventional scheme. By contrast, the mapping-demapping complexity is  $\mathcal{O}(k)$  for the proposed scheme, which is only linear in  $k$ . In the coded case, the conventional scheme includes two decoding processes to jointly decode  $\hat{s}_N$  and  $\hat{s}_F^N$  at UN, resulting in a high decoding complexity. The proposed scheme only involves a single decoding process to separately decode its own information  $\hat{s}_N$ , so that a low-complexity demapping-and-forward scheme can be used for the UF signal.

## VII. CONCLUSION

In this paper, we proposed a novel deep cooperative NOMA scheme to optimize the BER performance. We developed a new hybrid-cascaded DNN architecture to represent the cooperative NOMA system, which can then be optimized in a holistic manner. Multiple loss functions were constructed to quantify the BER performance, and a novel multi-task oriented two-stage training method was proposed to solve the end-to-end training problem in a self-supervised manner. Theoretical perspective was then established to reveal the learning mechanism of each DNN module. Simulation results demonstrate the merits of our scheme over OMA and the conventional NOMA scheme in various channel environments. As a main advantage, the proposed scheme can adapt to PA mismatch between training and inference, and can be incorporated with channel coding to combat signal deterioration. In our future work, we will consider the system designs for high-order constellations, transmission rate adaptation [43], and grant-free access [44], and to include more cooperative users [45], [46].

## APPENDIX

### A. Relationship among $\{L_1, L_2, L_3\}$

Demapping at UN is described as in (18), and  $\{L_1, L_2\}$  are the associated loss functions. The ultimate end-to-end demapping at UF is described in (21), and  $L_3$  is the associated end-to-end loss for the entire network. Let us observe (21). There are in total three random processes  $\{\mathcal{C}_{S,F}, \mathcal{C}_{N,F}, \mathcal{C}_{S,N}\}$  (due to

noise), while the remaining  $\{f'_S, f'_N, g'_N, g'_F\}$  are trainable modules.  $\{f'_S, f'_N, g'_N, g'_F\}$  are determined through training to combat the randomness from  $\{\mathcal{C}_{S,F}, \mathcal{C}_{N,F}, \mathcal{C}_{S,N}\}$ . We can see that to solve (21) exactly,  $\{h_{S,F}, h_{N,F}, h_{S,N}\}$  are all needed to describe  $\{\mathcal{C}_{S,F}, \mathcal{C}_{N,F}, \mathcal{C}_{S,N}\}$  correspondingly. However,  $h_{S,N}$  is practically not available at UF (recalling Section II-A), meaning that  $\mathcal{C}_{S,N}$  lacks description. This unavailable knowledge may potentially lead to a poor demapping performance. We further observe that conditioned on the case of  $\hat{\mathbf{s}}_F^N = \mathbf{s}_F$ , (21) can be described as

$$\begin{aligned} \hat{\mathbf{s}}_F &= g'_F(\mathcal{C}_{S,F} \circ f'_S(\mathbf{s}_N, \mathbf{s}_F), \mathcal{C}_{N,F} \circ \underbrace{f'_N}_{\text{Input: } \hat{\mathbf{s}}_F^N} \circ \underbrace{g'_N \circ \mathcal{C}_{S,N} \circ f'_S(\mathbf{s}_N, \mathbf{s}_F)}_{\text{Output: } (\hat{\mathbf{s}}_N, \hat{\mathbf{s}}_F^N)} | \hat{\mathbf{s}}_F^N = \mathbf{s}_F) \\ &= g'_F(\mathcal{C}_{S,F} \circ f'_S(\mathbf{s}_N, \mathbf{s}_F), \mathcal{C}_{N,F} \circ f'_N(\mathbf{s}_F) | \hat{\mathbf{s}}_F^N = \mathbf{s}_F), \end{aligned} \quad (40)$$

where the description of  $\mathcal{C}_{S,N}$  can be avoided. This observation inspires us to maximize  $\Pr\{\hat{\mathbf{s}}_F^N = \mathbf{s}_F\}$  to achieve (40) and solve (21) exactly with a high probability. It needs to be pointed out that the case  $\hat{\mathbf{s}}_F^N = \mathbf{s}_F$  means that the demapping (18) at UN succeeds for  $\mathbf{s}_F$  ( $L_2$  is sufficiently small). The above analysis reveals the causal structure between (18) and (21), which motivates us to perform optimization first for (18) and then for (21). Note that  $\Pr\{\hat{\mathbf{s}}_F^N = \mathbf{s}_F\}$  can be maximized (or equivalently,  $L_2$  can be minimized) through training stage I to achieve (40). Besides, considering the causal structure, in stage II, the modules learned from stage I, i.e.,  $f'_S$  and  $g'_N$ , are fixed.

### B. Derivations of (29) and (30)

First, (29) can be derived according to (28) by averaging over the channel output  $y_{S,N}$ . Then, by applying  $I_{f'_S}(\mathbf{S}_N(r), \mathbf{S}_F(r); Y_{S,N}) = I_{f'_S}(\mathbf{S}_N(r); Y_{S,N}) + I_{f'_S,2}(\mathbf{S}_F(r); Y_{S,N} | \mathbf{S}_N(r))$  from information theory and  $p_{f'_S}(\mathbf{s}_N(r) | y_{S,N}) = \int_{x_S} p_{f'_S}(\mathbf{s}_N(r) | x_S) p(x_S | y_{S,N}) dx_S$  from probability theory (to include the composite signal  $x_S$ ), (30) can be derived from (29).

### C. Proof of SINR Values for (35), (36), and (37)

Taking a closer look at (35) and (36), the respective inputs of  $g'_N(\cdot)$  can be written as

$$\frac{1}{\omega_N} y_{S,N} = h_{S,N} \left( \sqrt{\alpha_{S,N}} x_N + \frac{1}{\omega_N} \sqrt{\hat{\alpha}_{S,F}} x_F \right) + \frac{1}{\omega_N} n_{S,N}, \quad (41)$$

$$\frac{1}{\omega_F} y_{S,N} = h_{S,N} \left( \sqrt{\alpha_{S,F}} x_F + \frac{1}{\omega_F} \sqrt{\hat{\alpha}_{S,N}} x_N \right) + \frac{1}{\omega_F} n_{S,N}. \quad (42)$$

The SINRs can be calculated as  $\frac{\hat{\alpha}_{S,N} |h_{S,N}|^2}{\hat{\alpha}_{S,F} |h_{S,N}|^2 + 2\sigma_{S,N}^2}$  from (41) and  $\frac{\hat{\alpha}_{S,F} |h_{S,N}|^2}{\hat{\alpha}_{S,N} |h_{S,N}|^2 + 2\sigma_{S,N}^2}$  from (42). Similar proof can be given for (37).

## REFERENCES

- [1] M. Vaezi, Z. Ding, and H. V. Poor, *Multiple access techniques for 5G wireless networks and beyond*. Berlin, German: Springer, 2019.
- [2] Y. Liu, Z. Qin, and Z. Ding, *Non-Orthogonal Multiple Access for Massive Connectivity*. Switzerland: Springer, 2020.
- [3] Z. Ding, Y. Liu, J. Choi, Q. Sun, M. Elkashlan, I. Chih-Lin, and H. V. Poor, "Application of non-orthogonal multiple access in LTE and 5G networks," *IEEE Commun. Mag.*, vol. 55, no. 2, pp. 185–191, Feb. 2017.
- [4] L. Dai, B. Wang, Z. Ding, Z. Wang, S. Chen, and L. Hanzo, "A survey of non-orthogonal multiple access for 5G," *IEEE Commun. Surveys Tuts.*, vol. 20, no. 3, pp. 2294–2323, May 2018.
- [5] Z. Ding, M. Peng, and H. V. Poor, "Cooperative non-orthogonal multiple access in 5G systems," *IEEE Commun. Lett.*, vol. 19, no. 8, pp. 1462–1465, Aug. 2015.
- [6] J. Kim and I. Lee, "Capacity analysis of cooperative relaying systems using non-orthogonal multiple access," *IEEE Commun. Lett.*, vol. 19, no. 11, pp. 1949–1952, Nov. 2015.
- [7] Z. Wei, L. Dai, D. W. K. Ng, and J. Yuan, "Performance analysis of a hybrid downlink-uplink cooperative NOMA scheme," in *2017 IEEE 85th Vehicular Technology Conference (VTC Spring)*, Sydney, Australia, June 2017, pp. 1–7.
- [8] O. Abbasi, A. Ebrahimi, and N. Mokari, "NOMA inspired cooperative relaying system using an AF relay," *IEEE Wireless Commun. Lett.*, vol. 8, no. 1, pp. 261–264, Sep. 2019.
- [9] Y. Zhou, V. W. Wong, and R. Schober, "Dynamic decode-and-forward based cooperative NOMA with spatially random users," *IEEE Trans. Wireless Commun.*, vol. 17, no. 5, pp. 3340–3356, Mar. 2018.
- [10] Y. Liu, Z. Ding, M. Elkashlan, and H. V. Poor, "Cooperative non-orthogonal multiple access with simultaneous wireless information and power transfer," *IEEE J. Sel. Areas Commun.*, vol. 34, no. 4, pp. 938–953, Mar. 2016.
- [11] F. Kara and H. Kaya, "On the error performance of cooperative-NOMA with statistical CSIT," *IEEE Commun. Lett.*, vol. 23, no. 1, pp. 128–131, Jan. 2019.
- [12] —, "Error probability analysis of NOMA-based diamond relaying network," *IEEE Trans. Veh. Technol.*, vol. 69, no. 2, pp. 2280–2285, Feb. 2020.
- [13] Q. Li, M. Wen, E. Basar, H. V. Poor, and F. Chen, "Spatial modulation-aided cooperative NOMA: Performance analysis and comparative study," *IEEE J. Sel. Topics Signal Process.*, vol. 13, no. 3, pp. 715–728, Feb. 2019.
- [14] I. Goodfellow, Y. Bengio, and A. Courville, *Deep learning*. MIT press, 2016.
- [15] Z. Qin, H. Ye, G. Y. Li, and B.-H. F. Juang, "Deep learning in physical layer communications," *IEEE Wireless Commun.*, vol. 26, no. 2, pp. 93–99, Mar. 2019.
- [16] C. Zhang, P. Patras, and H. Haddadi, "Deep learning in mobile and wireless networking: A survey," *IEEE Commun. Surveys Tuts.*, vol. 21, no. 3, pp. 2224–2287, Mar. 2019.
- [17] H. He, S. Jin, C.-K. Wen, F. Gao, G. Y. Li, and Z. Xu, "Model-driven deep learning for physical layer communications," *IEEE Wireless Commun.*, vol. 26, no. 5, pp. 77–83, May 2019.
- [18] K. B. Letaief, W. Chen, Y. Shi, J. Zhang, and Y.-J. A. Zhang, "The roadmap to 6G: AI empowered wireless networks," *IEEE Commun. Mag.*, vol. 57, no. 8, pp. 84–90, Aug. 2019.
- [19] P. Dong, H. Zhang, G. Y. Li, I. S. Gaspar, and N. NaderiAlizadeh, "Deep CNN-based channel estimation for mmWave massive MIMO systems," *IEEE J. Sel. Topics Signal Process.*, vol. 13, no. 5, pp. 989–1000, July 2019.
- [20] H. He, C.-K. Wen, S. Jin, and G. Y. Li, "Model-driven deep learning for MIMO detection," *IEEE Trans. Signal Process.*, vol. 68, pp. 1702–1715, Feb. 2020.
- [21] Y. Lu, P. Cheng, Z. Chen, Y. Li, W. H. Mow, and B. Vucetic, "Deep autoencoder learning for relay-assisted cooperative communication systems," *IEEE Trans. Commun.*, 2020, early access.

- [22] T. O'Shea and J. Hoydis, "An introduction to deep learning for the physical layer," *IEEE Trans. Cogn. Commun. Netw.*, vol. 3, no. 4, pp. 563–575, Dec. 2017.
- [23] F. A. Aoudia and J. Hoydis, "Model-free training of end-to-end communication systems," *IEEE J. Sel. Areas Commun.*, vol. 37, no. 11, pp. 2503–2516, Nov. 2019.
- [24] N. Ye, X. Li, H. Yu, L. Zhao, W. Liu, and X. Hou, "DeepNOMA: A unified framework for NOMA using deep multi-task learning," *IEEE Trans. Wireless Commun.*, pp. 1–1, Jan. 2020.
- [25] N. Kato, B. Mao, F. Tang, Y. Kawamoto, and J. Liu, "Ten challenges in advancing machine learning technologies toward 6G," *IEEE Wireless Commun.*, vol. 27, no. 3, pp. 96–103, Apr. 2020.
- [26] M. Xu, F. Ji, M. Wen, and W. Duan, "Novel receiver design for the cooperative relaying system with non-orthogonal multiple access," *IEEE Commun. Lett.*, vol. 20, no. 8, pp. 1679–1682, June 2016.
- [27] N. Ye, A. Wang, X. Li, W. Liu, X. Hou, and H. Yu, "On constellation rotation of NOMA with SIC receiver," *IEEE Commun. Lett.*, vol. 22, no. 3, pp. 514–517, Dec. 2017.
- [28] J. N. Laneman, D. N. C. Tse, and G. W. Wornell, "Cooperative diversity in wireless networks: Efficient protocols and outage behavior," *IEEE Trans. Inf. Theory*, vol. 50, no. 12, pp. 3062–3080, Dec. 2004.
- [29] K. Deb and K. Deb, *Multi-objective optimization*. Boston, MA: Springer US, 2014, pp. 403–449.
- [30] S. Ruder, "An overview of multi-task learning in deep neural networks," *arXiv preprint arXiv:1706.05098*, 2017.
- [31] S. Dörner, S. Cammerer, J. Hoydis, and S. t. Brink, "Deep learning based communication over the air," *IEEE J. Sel. Topics Signal Process.*, vol. 12, no. 1, pp. 132–143, Feb. 2018.
- [32] T. M. Cover and J. A. Thomas, *Elements of information theory*. John Wiley & Sons, Nov. 2012.
- [33] Z. Popovic, "Amping up the PA for 5G: Efficient GaN power amplifiers with dynamic supplies," *IEEE Microw. Mag.*, vol. 18, no. 3, pp. 137–149, May 2017.
- [34] J. Sun, W. Shi, Z. Yang, J. Yang, and G. Gui, "Behavioral modeling and linearization of wideband RF power amplifiers using BiLSTM networks for 5G wireless systems," *IEEE Trans. Veh. Technol.*, vol. 68, no. 11, pp. 10348–10356, June 2019.
- [35] G. C. Clark Jr and J. B. Cain, *Error-correction coding for digital communications*. Springer Science & Business Media, 2013.
- [36] F. Alberge, "Deep learning constellation design for the AWGN channel with additive radar interference," *IEEE Trans. Commun.*, vol. 67, no. 2, pp. 1413–1423, Oct. 2018.
- [37] S. Cammerer, F. A. Aoudia, S. Dörner, M. Stark, J. Hoydis, and S. Ten Brink, "Trainable communication systems: Concepts and prototype," *IEEE Trans. Commun.*, June 2020.
- [38] L. Yuan, J. Pan, N. Yang, Z. Ding, and J. Yuan, "Successive interference cancellation for LDPC coded nonorthogonal multiple access systems," *IEEE Trans. Veh. Technol.*, vol. 67, no. 6, pp. 5460–5464, Apr. 2018.
- [39] H. Zheng, S. A. Hashemi, A. Balatsoukas-Stimming, Z. Cao, T. Koonen, J. Cioffi, and A. Goldsmith, "Threshold-based fast successive-cancellation decoding of polar codes," *arXiv preprint arXiv:2005.04394*, 2020.
- [40] T. Sypherd, M. Diaz, L. Sankar, and P. Kairouz, "A tunable loss function for binary classification," in *2019 IEEE International Symposium on Information Theory (ISIT)*, Paris, France, July 2019, pp. 2479–2483.
- [41] M. Chen, U. Challita, W. Saad, C. Yin, and M. Debbah, "Artificial neural networks-based machine learning for wireless networks: A tutorial," *IEEE Commun. Surveys Tuts.*, vol. 21, no. 4, pp. 3039–3071, July 2019.
- [42] S. S. U. Ghouri, S. Saleem, and S. S. H. Zaidi, "Enactment of LDPC code over DVB-S2 link system for BER analysis using MATLAB," in *Advances in Computer Communication and Computational Sciences*, S. K. Bhatia, S. Tiwari, K. K. Mishra, and M. C. Trivedi, Eds. Singapore: Springer, 2019, pp. 743–750.
- [43] B. Makki, T. Svensson, and M. Zorzi, "An error-limited NOMA-HARQ approach using short packets," *arXiv preprint arXiv:2006.14315*, 2020.
- [44] L. Liu, E. G. Larsson, W. Yu, P. Popovski, C. Stefanovic, and E. de Carvalho, "Sparse signal processing for grant-free massive

connectivity: A future paradigm for random access protocols in the Internet of Things,” *IEEE Signal Process. Mag.*, vol. 35, no. 5, pp. 88–99, Sep. 2018.

- [45] X. Wu, A. Ozgur, M. Peleg, and S. S. Shitz, “New upper bounds on the capacity of primitive diamond relay channels,” in *2019 IEEE Information Theory Workshop (ITW)*, Visby, Sweden, Aug. 2019, pp. 1–5.
- [46] N. Wu, X. Zhou, and M. Sun, “Incentive mechanisms and impacts of negotiation power and information availability in multi-relay cooperative wireless networks,” *IEEE Trans. Wireless Commun.*, vol. 18, no. 7, pp. 3752–3765, July 2019.